The Astrophysical Journal, 679:925–941, 2008 June 1

HOW THE FIRST STARS REGULATED LOCAL STAR FORMATION. I. RADIATIVE FEEDBACK

Daniel Whalen,[1] Brian W. O'Shea,[1,2] Joseph Smidt,[3] and Michael L. Norman[4]
Received 2007 August 12; accepted 2008 February 16

ABSTRACT

We present numerical simulations of how a 120 $M_\odot$ primordial star regulates star formation in nearby cosmological halos at $z \sim 20$ by photoevaporation. Our models include nine-species primordial chemistry and self-consistent multi-frequency conservative transfer of UV photons with all relevant radiative processes. Whether or not new stars form in halos clustered around a Population III star ultimately depends on their core densities and proximity to the star. Diffuse halos with central densities below 2–3 cm^{-3} are completely ionized and evaporated anywhere in the cluster. Evolved halos with core densities above 2000 cm^{-3} are impervious to both ionizing and Lyman-Werner flux at most distances from the star and collapse as quickly as they would in its absence. Star formation in halos of intermediate density can be either promoted or suppressed depending on how the ionization front (I-front) remnant shock compresses, deforms, and enriches the core with H_2. We find that the 120 $M_\odot$ star photodissociates H_2 in most halos in the cluster, but that catalysis by H^- restores it a few hundred kiloyears after the death of the star, with little effect on star formation. Our models exhibit significant departures from previous one-dimensional, spherically symmetric simulations, which are prone to serious errors due to unphysical geometric focusing effects.

Subject headings: cosmology: theory — early universe — H II regions

1. INTRODUCTION

Radiative feedback of one generation of stars on the next has regulated the rise of stellar populations since the birth of the first luminous objects in the universe. In the ΛCDM paradigm of hierarchical structure formation, small dark matter halos at high redshifts assembled into larger structures by collisions and mergers. When the first pregalactic objects reached masses of $\sim 1.0 \times 10^5$ $M_\odot$ at $z \sim 50$, molecular hydrogen cooling allowed primordial gas in them to collapse and form the first stars. Numerical simulations indicate that these stars formed in isolation (one per halo) and, due to the inefficiency of H_2 cooling, were likely very massive, from 15 to 500 $M_\odot$ (Abel et al. 2000, 2002; Bromm et al. 1999; O'Shea & Norman 2007). With surface temperatures in excess of 100,000 K, many of these Population III stars were millions of times more luminous than the Sun and prodigious sources of both ionizing and Lyman-Werner (LW) ultraviolet (UV) radiation. LW photons in the 11.18–13.6 eV energy range on average dissociate 15% of the H_2 molecules they encounter through excitation to electronic states that decay to the vibrational continuum. Radiation hydrodynamical calculations indicate that the H II regions of Population III stars were up to 10 kpc in diameter, with strong mass outflows capable of evicting half of the baryons from their halos (Whalen et al. 2004; Kitayama et al. 2004; Alvarez et al. 2006; Abel et al. 2007; Johnson et al. 2007; Yoshida et al. 2007; Wise & Abel 2007c). The transparency of neutral H and He to LW photons allowed them to propagate farther into the early universe than ionizing UV, dissociating H_2 far beyond the H II region.

When halos grew to greater masses they could instead cool by atomic H line emission. These structures hosted the first small star populations by $z \sim 12$–15. Although the initial mass function (IMF) of these stars remains unknown (having never been simulated or constrained observationally), it is thought that protogalaxies shouldered the bulk of cosmological reionization from $z \sim 8$ to 15 (Ricotti et al. 2001; Ciardi et al. 2003). Thus, over time the first stars and galaxies gradually built up both an ionizing and LW dissociating UV background in the intergalactic medium (IGM).

A key question in cosmological reionization and structure formation is how radiation from one generation of stars influenced the next. In global models of cosmological evolution that average over the fine structure of reionization, it has been suggested that the H II regions of the first stars and galaxies created an "entropy floor" in which later star formation was discouraged (Oh & Haiman 2003). On the other hand, numerical studies demonstrate that molecular hydrogen in the ionization fronts (I-fronts) of protogalaxies (Ricotti et al. 2001) enhanced gas cooling in the early IGM, thereby promoting star formation. Photons from hard UV sources exhibit a range of mean free paths in prefront gas that broaden the I-front. Substantial free electron fractions at only a few thousand kelvins can be established in the outer layers of these fronts, catalyzing H_2 formation on timescales much shorter than the dynamical times of the H II region. These scenarios are known as negative and positive radiative feedback, respectively.

A rising LW background may have suppressed star formation in low-mass halos, sterilizing them of molecular hydrogen needed for dynamical collapse. Machacek et al. (2001) performed numerical simulations of pregalactic structure evolution in the presence of a uniform LW background and discovered that star formation was delayed rather than prevented. They found that as halos grew and their central densities rose, their cores became self-shielded from the background, permitting the formation of H_2 and their eventual cooling and collapse. Machacek et al. (2003) later examined the effect of soft X-ray backgrounds due to early populations of miniquasars (Kuhlen & Madau 2005) on structure formation. X-ray spectra may partially ionize pregalactic clouds without raising them to high temperatures, creating favorable conditions for H_2 formation and cloud collapse. However, this effect was found to be relatively mild for a wide range of X-ray backgrounds, with molecular hydrogen concentrations still being determined by the equilibrium between H_2 catalysis and LW dissociation. These

[1] Applied Physics (X-2), Los Alamos National Laboratory, Los Alamos, NM 87545; dwhalen@lanl.gov.
[2] Theoretical Astrophysics (T-6), Los Alamos National Laboratory.
[3] Department of Physics and Astronomy, Brigham Young University, Provo, UT 84602.
[4] Center for Astrophysics and Space Sciences, University of California at San Diego, La Jolla, CA 92093.

numerical calculations were both performed in cosmological simulation volumes (1 Mpc^3 comoving). O'Shea & Norman (2008) and Wise & Abel (2007a, 2007b) have recently revisited primordial star formation in strong LW backgrounds in somewhat smaller cosmological volumes.

Recently, studies have turned to the suppression or promotion of star formation on small scales in cosmological halos proximate to the first stars. These surveys sacrifice radiation transport to follow the collapse of the halo into a new star. The first in this vein was O'Shea et al. (2005), who considered a minihalo assumed to be "flash ionized" (ionized on timescales much shorter than outflow times) by a 120 $M_\odot$ Population III star. They found molecular hydrogen to readily form in the warm relic H II region, causing rapid cooling of the halo and formation of a primordial star. The main limitation of this study was its neglect of the evaporation and photodissociation of the halo itself, so its final state was open to debate. Yoshida et al. (2007) revisited local UV feedback in a broader range of environments and included HD cooling. They found second-generation star formation to be highly situational; when collapse did occur, HD cooling led to fragmentation on smaller mass scales and stars significantly smaller than their progenitors. More ambitious numerical attempts have been made to assemble the first primeval galaxies by the consecutive formation of primordial stars, one often in the relic H II region of its predecessor (Johnson et al. 2007; Yoshida et al. 2007). In these models, which emphasize the role of radiative feedback in protogalaxy evolution, star formation in remnant ionization fields is weakly suppressed and, due to HD cooling, led again to a less massive generation of stars.

The latest experiments abandon collapse of the halo into a star and focus instead on its dissociation and evaporation, inferring the likelihood of star formation from its final state. Susa & Umemura (2006) performed radiation smoothed particle hydrodynamical (RSPH) calculations of the ionization of a clump residing in the same halo as a primordial star. Accounting for both photodissociation and ionization, they discovered a threshold density of 100 cm^{-3} above which the clump could still collapse, even when the star was at 30 pc. Central densities greater than this were sufficient to self-shield the core of the cloud from the LW flux of the star. H_2 forming in the I-front also protected molecular hydrogen in the cloud from destruction during photoevaporation. Below these densities the radiation front generally overran the halo, dispersing the gas into the IGM. In a numerical suite by Susa (2007), halos with central densities above 1000 cm^{-3} self-shield from reasonable values of metagalactic backgrounds as well.

The most complete survey to date of primordial halo evaporation for a grid of masses and UV fluxes was by Ahn & Shapiro (2007, hereafter AS07), who found local radiative feedback to be mostly neutral. In short, halos destined to collapse into stars would still do so in the presence of the UV source, while those too small to form stars would be prevented from doing so by the radiation. They identified a novel mechanism of cloud collapse due to shock-induced molecule formation (SIMF). AS07 found that the D-type I-front shock sometimes accelerated at the center of the halo, heating it above 10,000 K and collisionally ionizing it. Abrupt H_2 formation ensued, causing a cooling pulse leading to rapid collapse of the core and creation of a star.

Unfortunately, this well-parameterized study is problematic because of its choice of coordinate mesh. The semianalytical halos adopted in their calculations were centered in a one-dimensional spherical Lagrangian grid, with incoming radiation from the outer boundary. In three dimensions this arrangement corresponds to a radially symmetric halo bathed by a centrally directed field from all angles rather than the more realistic radiation wave that would sweep over an actual halo from one direction. Two unphysical effects result from such implosion geometries. First, as matter is crushed inward uniformly from all directions it rises to much higher densities than if compressed from one side, causing the D-type shock to become much stronger than in an actual photoevaporating halo. This leads to the artificial heating and collisional ionization of the core evident in many of the AS07 models and overestimates the degree to which shocks penetrate the core. Second, placing the core on the inner boundary guarantees that shocks reaching the center will rebound, in contrast to the one-sided compression and displacement of the core that really occurs. Both effects lead to serious departures from the true evolution of the halo once the shock is within 10 pc of the core, rendering many of the authors' findings suspect.

We present a suite of two-dimensional axisymmetric radiation hydrodynamical calculations of the ionization and photodissociation of cosmological minihalos by a 120 $M_\odot$ star. Our initial conditions are spherically averaged halos derived from cosmological initial conditions with the Enzo adaptive mesh refinement (AMR) code. The baryon profiles chosen for this study are a series of snapshots of the same halo taken at different redshifts to evaluate the impact of the I-front on the halo at any of its evolutionary stages at several distances from the UV source. The aim of this survey is to span the range of possibilities for local radiative feedback in the first generation of luminous objects in the universe. Consequently, we do not consider the contributions of metagalactic LW or X-ray backgrounds here but reserve these effects for later study. An auxiliary objective is to evaluate the degree to which photoevaporation of star-forming clouds is distorted in spherical geometry, a practice not limited to AS07 (Bertoldi 1989; Bertoldi & McKee 1990; Cen 2001).

In § 2 of this paper we evolve a semianalytical halo from AS07 with radiation in our two-dimensional geometry for comparison to the one-dimensional result. This study illustrates the sequence of events in halo dissociation and evaporation, which is explored in § 3. There we motivate our choice of halo profiles and illuminating fluxes, tabulate final outcomes for each model, and review the range of possibilities for radiative feedback in the cluster. In § 4 we conclude.

2. TIS HALO PHOTOEVAPORATION

The semianalytical truncated isothermal sphere (TIS) halo model from AS07 we test here is $2.0 \times 10^5\ M_\odot$, located 540 pc from a 120 $M_\odot$ star. TIS halos are reasonable approximations of the density profile of a cosmological halo and are parameterized by their truncation radius r_t (or outer boundary),

$$r_t = 102.3\left(\frac{\Omega_0}{0.27}\right)^{-1/3}\left(\frac{h}{0.7}\right)^{-2/3} \times \left(\frac{M}{2.0\times10^5\ M_\odot}\right)^{1/3}\left(\frac{1+z}{1+20}\right)^{-1}\ \mathrm{pc}, \quad (1)$$

their virial temperature,

$$T = 593.5\left(\frac{\mu}{1.22}\right)\left(\frac{\Omega_0}{0.27}\right)^{1/3}\left(\frac{h}{0.7}\right)^{2/3} \times \left(\frac{M}{2.0\times10^5\ M_\odot}\right)^{2/3}\left(\frac{1+z}{1+20}\right)\ \mathrm{K}, \quad (2)$$

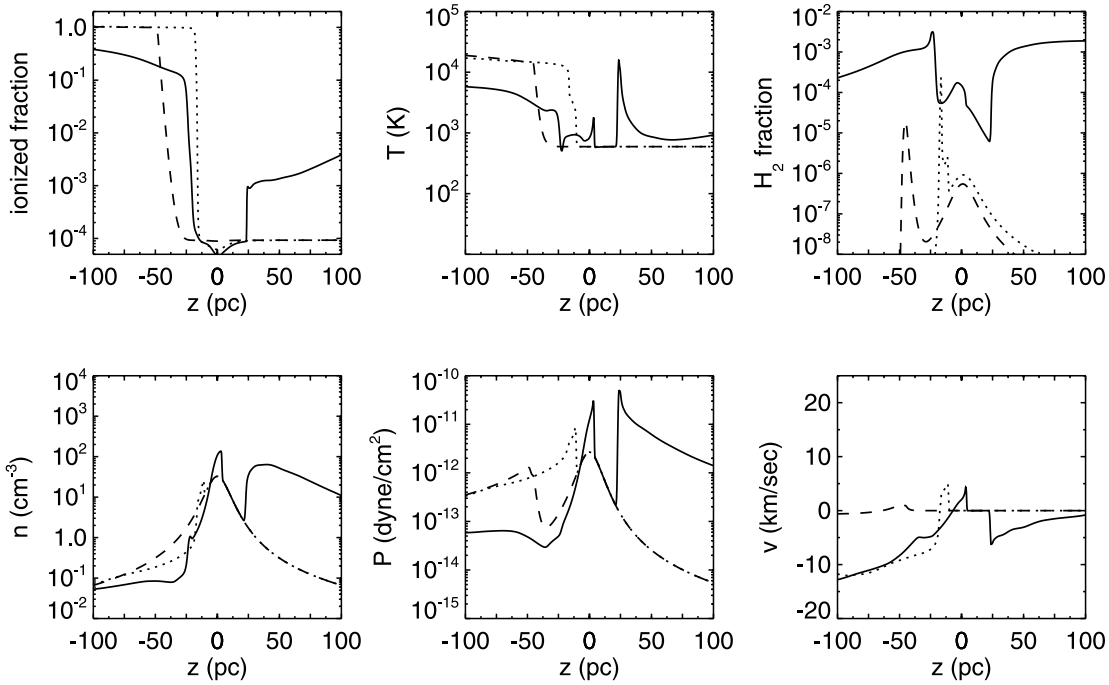

FIG. 1.—Ionized fraction, density, temperature, pressure, H_2 fraction, and velocity profiles in the TIS halo. *Dashed lines*: 200 kyr; *dotted lines*: 2.4 Myr; *solid lines*: 4.5 Myr.

and their central density,

$$\rho_0 = 4.144 \times 10^{-22} \left(\frac{\Omega_0}{0.27}\right)\left(\frac{h}{0.7}\right)^2 \times \left(\frac{1+z}{1+20}\right)^3 \text{ g cm}^{-3}. \quad (3)$$

The halo density profile as a function of radius is given by

$$\rho(r) = \left(\frac{a_1}{a_2+\xi^2} - \frac{b_1}{b_2+\xi^2}\right)\rho_0, \quad (4)$$

where $a_1 = 21.38$, $a_2 = 9.08$, $b_1 = 19.81$, $b_2 = 14.62$, and $\xi = r/(r_t/29.4)$ from equations (103) and (104) of Shapiro et al. (1999).

We model the evaporation of this halo with ZEUS-MP (Whalen & Norman 2006, 2008a), a massively parallel Eulerian reactive flow hydrocode with self-consistent multifrequency photon-conserving UV radiative transfer (Whalen & Norman 2008b), and the nine-species primordial gas reaction network of Anninos et al. (1997). We have ported our algorithm to ZEUS-MP 2.0, the recent F90 public release of the code capable of performing calculations in one, two, or three dimensions in Cartesian (XYZ), cylindrical (ZRP), or spherical (RTP) coordinate meshes (Hayes et al. 2006). Our photon-conserving transport, separate from the flux-limited diffusion (FLD) native to ZEUS-MP, can simulate photons from a point source centered in a spherical grid or plane waves along the x- or z-axes of Cartesian or cylindrical boxes. Depending on the dimensionality and type of coordinate mesh, the code can apply spherical shell, conjugate gradient (CG), or multigrid methods to solve Poisson's equation for the self-gravity of the gas.

We centered the TIS halo at the origin of a two-dimensional axisymmetric cylindrical (ZR) coordinate box, with boundaries of -125 and 125 pc in z, and 0.01 and 125 pc in r. The grid was discretized into 1000 zones in z and 500 zones in r for a spatial resolution of 0.25 pc. Outflow conditions were applied to the upper and lower z boundaries, and reflecting and outflow conditions were assigned to the inner and outer boundaries in r, respectively. The gas was primordial, 76% H and 24% He by mass. The gravitational potential of the dark matter was included by computing the potential necessary to cancel pressure forces everywhere on the grid (setting the halo in hydrostatic equilibrium) and holding this potential fixed throughout the simulation. Excluding dark matter dynamics introduces no significant errors, because the gas in the halo evolves on much shorter timescales than either the Hubble time or merger timescales. Updates to the self-gravity of the gas were performed every hydrodynamical time step by solving Poisson's equation with a two-dimensional CG solver. Cooling by electron collisional excitation and ionization, recombination, bremsstrahlung, and inverse Compton scattering of the cosmic microwave background (CMB), assuming a redshift $z = 20$, was present in all the models. H_2 cooling was also included using the cooling curves of Galli & Palla (1998).

We partition photon emission rates by energy into 40 uniform bins from 0.755 to 13.6 eV, and 80 logarithmically spaced bins between 13.6 and 90 eV according to the blackbody spectrum of the 120 $M_\odot$ star. The rates are normalized by the total number of ionizing photons emitted per second by the star from Schaerer (2002). Photons in the lower energy range cannot ionize H or He but do drive a host of chemical reactions that regulate H^- and H_2 formation and are tabulated in Table 1 of Whalen & Norman (2008b). H_2 photodissociation rates are computed with the self-shielding functions of Draine & Bertoldi (1996), modified for thermal doppler broadening as in AS07 to account for gas flows. The legitimacy of thermal broadening as a proxy for flows in evaporating halos is uncertain, but including it reduces shielding at intermediate column densities, setting upper limits on H_2 dissociation. We attenuate the intensity of the plane wave by $1/R^2$ to approximate geometrical dilution of the radiation. The cloud is irradiated for 2.5 Myr, the main-sequence lifetime of the 120 $M_\odot$ star, and then left to evolve in the relic H II region for another 2.5 Myr.

As a control we chemothermally evolved the halo for 4.8 Myr without radiation to determine the degree to which the core cools and condenses in the absence of stellar feedback. Although $e-$ and

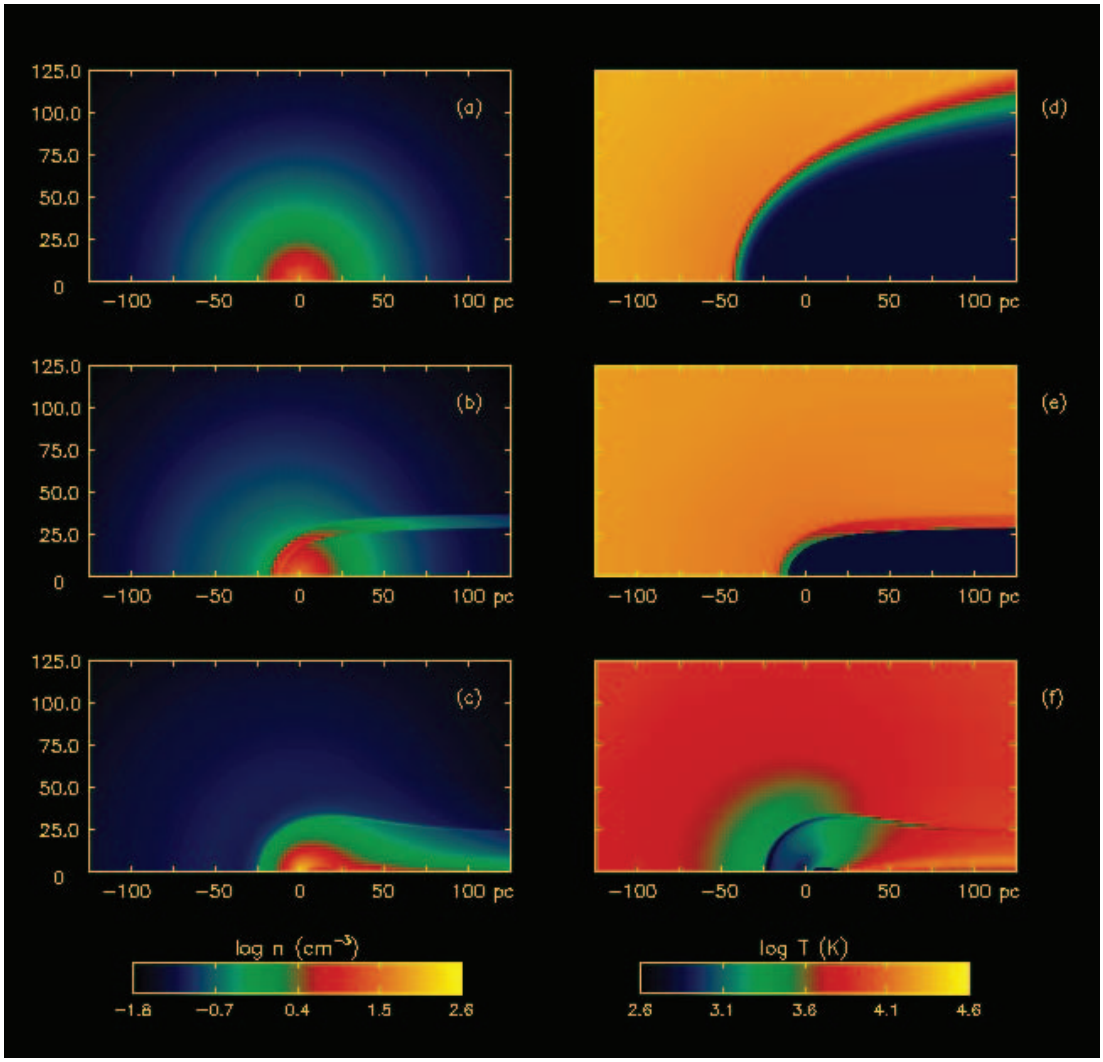

FIG. 2.—Photoevaporating TIS halo. Panels (*a*), (*b*), and (*c*) are densities at 200 kyr, 2.4 Myr, and 4.5 Myr, respectively. Panels (*d*), (*e*), and (*f*) are temperatures at 200 kyr, 2.4 Myr, and 4.5 Myr, respectively. In this and all other color figures in the paper, the horizontal axis is *Z* and the vertical axis is *R*.

H_2 fractions are initially uniform throughout the cloud, H_2 catalysis and cooling follows the density profile and is greatest in the core where the density peaks. Cooling disrupts the pressure balance with gravity, and the core begins to contract. As densities rise, so do molecular hydrogen production and cooling, and the collapse accelerates. In this halo infall is leisurely, and we find that central densities only change from 31 to 36 cm^{-3} in 4.8 Myr, consistent with what was found in AS07. The self-gravity of the gas is essential to this process; if deactivated, little gas motion occurs on these timescales. AS07 find that if collapse proceeds undisturbed a star forms in this halo at 32 Myr, so it is an appropriate candidate for radiative feedback.

2.1. *The R-Type Front*

We show ionized fraction, number density, temperature, pressure, H_2 fraction, and velocity profiles along the *z*-axis through the center of the TIS halo at three times in Figure 1. Figures 2 and 3 are images of the densities, temperatures, and H_2 fractions on the grid for the same three times. The I-front enters the lower *z* face of the box at $t = 0$. The absence of shock plateaus in the abrupt temperature and pressure profiles together with the undisturbed densities at 200 kyr indicate that the front is R-type. LW photons ahead of the front dissociate molecular hydrogen both in the core and beyond, as seen in the sudden displacement downward of the H_2 profile from 2.0×10^{-6} by $t = 200$ kyr. There are two peaks in this curve, one at -50 pc and one at the core. The first (2×10^{-5}) is H_2 in the outer layer of the I-front, whose partial ionization and moderate temperatures facilitate its formation. As discussed below, this H_2 layer eventually acts as a shutter, preventing LW flux from the star from reaching the core.

The second peak is the equilibrium H_2 abundance ($\sim 6 \times 10^{-7}$) set in the core by a balance between LW dissociation and formation through the H^- channel. Equilibrium fractions fall beyond the core because the large central densities replenish H_2 at greater rates than in the more tenuous outer envelope. Molecular hydrogen fractions ahead of the front remain stable while it is R-type but begin to rise when it becomes D-type at $\simeq$30 pc. The front is broad in the diffuse IGM densities 50 pc from the center of the halo ($\sim$25 pc at 200 kyr) due to the spread of mean free paths in the hard UV tail of the 100,000 K blackbody spectrum. It narrows and slows as it ascends the density gradient toward the core of the cloud.

Figures 2*d* and 3*a* reveal the cometary appearance of the front at 200 kyr due to its preferential advance in the stratified layers above and below the halo. This parabolic shadow, common to all our models, is predicted analytically using inverse Strömgren layer arguments (§ 2.3.2 of Shapiro et al. 2004). Molecular hydrogen in the R-type front extends in a yellow arc from the *z*-axis

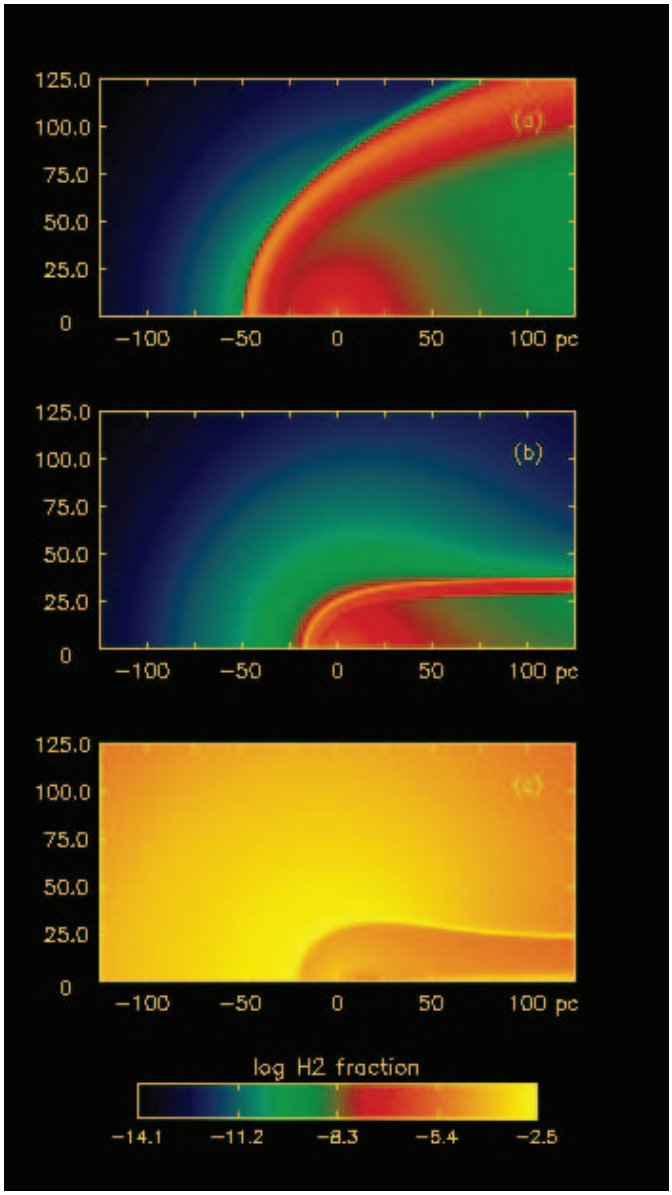

FIG. 3.—H_2 fractions in the photoionized TIS halo; panels (*a*), (*b*), and (*c*) are at 200 kyr, 2.4 Myr, and 4.5 Myr, respectively.

out to the end of the box on the right in Figure 3*a*. The reddish hues of the higher equilibrium H_2 fractions within the halo stand out against the greenish hues of the lower fractions in the diffuse envelope. The densities remain largely unchanged because the front is still supersonic.

2.2. *The D-Type Front*

As the front slows, a pressure wave builds in the ionized gas, pushing past the front and steepening into a shock. This marks the transformation of the front to D-type and the onset of photoevaporation. The shock soon detaches from the front, as shown in the $t = 2.4$ Myr temperature plot in Figure 1. The gas drops sharply in temperature from 20,000 to 3000 K from ionized to shocked gas. The neutral shell extends a few parsecs to the shock where the temperature again drops, this time to the background. The shocked shell is the sharp peak to the left of $z = 0$ in the density profile at 2.4 Myr. As the front approaches the center of the cloud, ionized backflow to the left is visible in the velocity profile at 2.4 Myr. This photoevaporated gas exits at 5–10 km s^{-1}, well above the 2–3 km s^{-1} escape velocity of the halo, and does not return unless recaptured by mergers, whose timescales at $z \sim 20$ are $\sim$20 Myr. The shock is 13 pc from the core at a velocity of 5 km s^{-1} when the star exits the main sequence.

The high-energy photons in the front encounter greater densities as they penetrate the neutral shocked shell. The electrons they liberate catalyze molecular hydrogen formation at the base of the shell, elevating H_2 fractions there to 3.0×10^{-4}. As the D-type front advances from -30 to -25 pc, molecular hydrogen fractions in the halo steadily rise and then level off as they come to new equilibrium values, being partially shielded from the LW flux. Core H_2 fractions reach 1.0×10^{-6} and remain there until the death of the star. As molecular hydrogen levels rise, temperatures in the core fall from 600 to 400 K. This modest restoration of H_2 falls short of the original fraction that was dissociated. The initial free electron fraction on the grid (which drives H_2 formation at the center) is slowly depleted by recombinations as the halo evolves. Recombinations are faster in the higher densities of the core, producing the dip in ionized fraction there at 2.4 Myr. Note that in the halo beyond the front the H_2 fraction generally follows the density profile, as one would expect.

In Figure 2*e* the partially evaporated halo casts a nearly cylindrical shadow along the *z*-axis by the time the Population III star dies. Ionized gas surrounding the shadow drives an axial implosion shock toward the axis. The ablation shock approaching the halo is the green parabola that begins on the axis and narrows outward along the arc in the temperature image. H_2 cooling is visible in the core as the circular blue patch at the center of the mesh; corresponding elevated molecular hydrogen concentrations are visible in yellow in Figure 3*b*. Densities are greatest in the shock and the center of the cloud in Figure 2*b*. The cometary shocked shell being driven toward the axis is the thin layer of green and aqua parallel to the *z*-axis. At 2.4 Myr the left hemisphere of the cloud has been largely photoevaporated, and the inner part of the halo is compressed to the right.

2.3. *The Relic* H II *Region*

The H II region begins to recombine when the 120 $M_\odot$ star dies at 2.5 Myr, most likely by direct collapse to a black hole (Heger et al. 2003). H_2 formation becomes explosive in the warm relic ionization field and shock, which continues into the core as it slows. As ionized gas surrounding the shadow of the halo cools some pressure support for the shock is lost, but it still converges on the *z*-axis. After the death of the star a rarefaction wave develops in the opposite direction just behind the shock and retreats to -37 pc by 4.5 Myr, as seen in the dip in pressure there in Figure 1.

At 4.8 Myr the shock, highly enriched with molecular hydrogen, merges with the core. The central density rises to 398 cm^{-3}, more than 10 times its original value, with an H_2 fraction of 3.0×10^{-3}. In the absence of any radiation this core would have chemothermally evolved to a central density of only 36 cm^{-3}. While both density and H_2 have been greatly enhanced by the radiation, the gas is moving at 5 km s^{-1}. Although it will likely slow below 2–3 km s^{-1} and become gravitationally bound to the halo, it is unclear if a star will form in this gas.

The cylindrical shock converges symmetrically on the *z*-axis on all azimuths, heating to over 10,000 K and becoming collisionally ionized to the right of the coordinate origin in the 4.5 Myr temperature and ionized fraction profiles. A surge in molecular hydrogen production follows along the central axis, visible in both the H_2 fraction plot for $z > 25$ pc and Figure 3*c*. The shock converges on the axis first in the lower densities beyond the core; as gas closer to $z = 0$ reaches the axis, a reverse shock builds toward the halo in the negative *z*-direction, as shown in the velocity

profile at 4.5 Myr. This shock drives material back into the halo but is still 25 pc from the core at 4.8 Myr. The pulse of H_2 formation is the SIMF found by AS07 in many of their models. Actual halos have morphologies that would break simultaneous convergence of gas onto the axis and probably avoid SIMF.

When the H II region begins to recombine, the ionized backflow to the left of the halo is at first isothermal, with a density gradient that falls with distance. The isothermal equation of state mandates pressure gradients wherever there are density drops, and these pressures accelerate the backflow even as the gas recombines, as shown in the 4.5 Myr velocities for $z < 0$. Also, the lowest temperatures at later times are just behind the shock remnant merging with the core from the left; these correspond to the pressure minimum and are due to $P\,dV$ work done by the rarefaction wave receding from the core. In general, temperatures and ionization fractions drop fastest where densities are greatest, as in these plots.

The density and temperature images in Figures 3*c* and 3*f* reveal the slight displacement of the core to the right of the coordinate center by the remnant shock at 4.5 Myr. A reflection shock from the axis beyond $z = 25$ pc collides with partially ionized gas still driven inward. The warm relic H II region encircles the eroded halo in teardrop density contours, and the shock, now cooled to 160 K, appears as a single large tail curled around the cool dense halo core. Molecular hydrogen production radiates outward from the core in a yellow arc that dims slightly with distance from the center of the mesh in Figure 3*c*. This is due to the density dependence of H_2 formation rates: production erupts first in the core, following later in the more diffuse outer envelope.

We note that a more realistic point source of radiation situated on the *z*-axis would cast a parabolic shadow like the one at later times in the Susa & Umemura (2006) calculations rather than the cylindrical shadow in our simulations. However, recombination photons, excluded in our models by the on-the-spot approximation, may compensate by photoionizing gas toward the central axis. A shock would still be driven into the shadow, narrowing it to a greater degree than in point-source simulations that ignore reprocessed radiation but perhaps not to the extent in UV plane wave geometries like ours. The shadow becomes increasingly cylindrical with point sources at greater distances.

2.4. *Consequences of One-Dimensional Geometries*

Figure 1 of Whalen & Norman (2008b) and Figure 8 of AS07 illustrate the general agreement that would be expected between the two models while the front is far from the core, supersonic and still free of curvature effects. The fraction profiles for all nine species indicate that both codes predict the same position for the front at $t = 0.6t_*$, where t_* is the main-sequence lifetime of the star. Furthermore, in both studies the I-front becomes fully D-type $\sim$25 pc from the center of the halo and is 10–12 pc from the core when the star dies.

As matter closes in on the core from all sides in the AS07 code the two solutions begin to diverge. When the shock in the one-dimensional code reaches the density plateau near the center it actually accelerates, which would not occur in a core compressed from one side. In our two-dimensional simulations the shock gradually decelerates from 7.5 to 5 km s^{-1} as it penetrates the core. Disagreement between the two models becomes acute as the shock artificially heats and collisionally dissociates the core in the Lagrangian code. A cascade of thermal events at the center of the cloud follows, ending in spurious runaway collapse. Rapid H_2 formation follows collisional ionization, in turn driving excessive cooling that leads to isothermal jump conditions in the shock remnant. The density jump in the remnant rises to very high values that further accelerate cooling and collapse.

The velocity of the shock in our model tapers as the rarefaction wave drains it of pressure support, and it snowplows gas in the core. Densities rise when the remnant reaches the core, but not to the degree associated with the artificial cooling and compression in the one-dimensional calculation. H_2 fractions rise at the center because of mixing with molecular hydrogen accumulated in the remnant and formation by in situ H^- rather than collisional ionization by an enhanced shock. Radiative feedback in the end result is unclear, unlike the severe positive feedback predicted by AS07.

Contrary to the claim of AS07, the bounce of the shock from the inner reflecting boundary in their model cannot be equated to a planar shock interacting with the central density peak. The remnant instead displaces the gas at the center without the rebound associated with core bounce. Our model thus avoids the unphysical delays in core collapse that follow from the reflection of the shock at the center of the AS07 models.

We emphasize that these difficulties are not unique to AS07 but are general to one-dimensional spherically symmetric models of the external photoevaporation of star-forming clouds (Bertoldi 1989; Bertoldi & McKee 1990; Cen 2001).

3. TWO-DIMENSIONAL ENZO MODELS

The initial conditions used in our two-dimensional calculations are taken from a simulation performed with Enzo, a publicly available, extensively tested AMR cosmology simulation code (O'Shea et al. 2004). The details of this calculation (and others in the series) are described in detail in O'Shea & Norman (2007) but are summarized here for clarity. We select one calculation from the suite of 12 in O'Shea & Norman (2007), choosing simulation L0_30D since it has the smallest halo mass at the epoch of collapse ($1.35 \times 10^5\ M_\odot$). Here, the epoch of collapse is defined to be the redshift in the simulation at which gas in the given halo has collapsed to central densities for which star formation is inevitable. This simulation was initialized at $z = 99$ in a cosmological volume 300 h^{-1} kpc (comoving) on a side, with a 128^3 root grid and three static nested grids, and an effective resolution of 1024^3 cells/particles on the highest level static grid. This corresponds to a dark matter (gas) resolution of $2.60(0.40)\,M_\odot$. The highest level static nested grid is large enough to contain the entire Lagrangian volume, which will end up within the virial radius of the final halo, ensuring that the halo is resolved by approximately 5×10^4 dark matter particles and a comparable number of cells for the equations of hydrodynamics.

This calculation is then evolved from $z = 99$ until the collapse of the most massive halo in the simulation following the equations of dark matter dynamics, hydrodynamics, and a nine-species nonequilibrium primordial chemistry model (Abel et al. 1997; Anninos et al. 1997). We employ a maximum of 28 levels of AMR, until the gas at the center of the halo cools and collapses to high ($n_{\rm H} > 10^8$ cm^{-3}) densities at $z = 24.74$. Cells are refined on a variety of criteria, including dark matter and baryon density, cooling time, Jeans length, and shock and energy gradient resolution. In addition, mass is refined in a super-Lagrangian way, such that the gas mass resolution at the maximum level of refinement is $m_{\rm cell} \simeq 10^{-3}\ M_\odot$. Data are output periodically throughout the simulation, and then more rapidly during the collapse of the gas in the halo, such that one output is generated every time the central halo density increases by a factor of 8. One-dimensional profiles are then created by finding the cell with the highest baryon density in the collapsed halo core and taking mass-weighted spherical averages of baryon density, temperature, and other

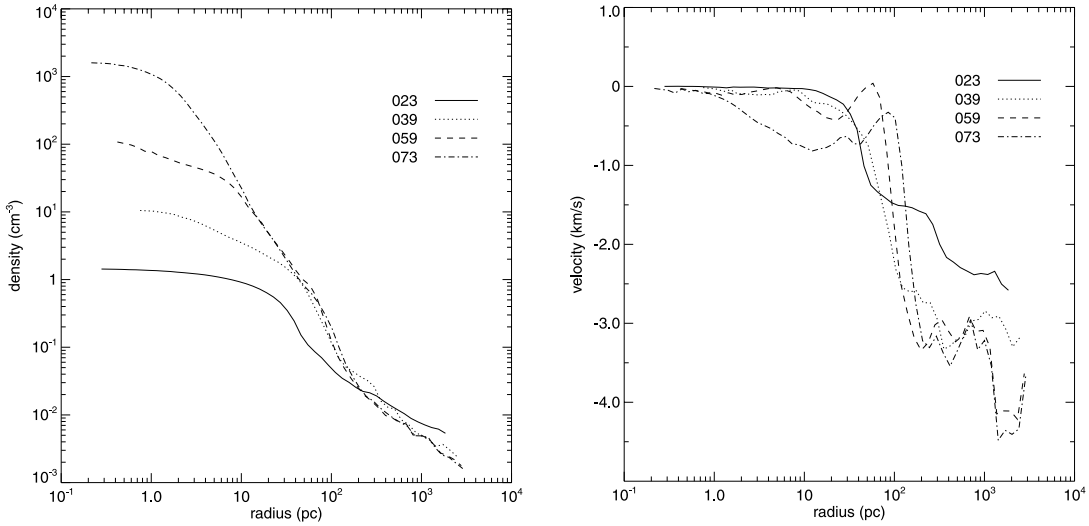

FIG. 4.—Four halo profiles. The redshifts of the 023, 039, 059, and 073 profiles are 23.9, 17.7, 15.6, and 15.0, respectively. *Left*: Densities. *Right*: Radial velocities.

quantities. We use logarithmic bins so that the spatial extent of the bins in the radial profile always approximates the cell resolution at any given radius. Four of these spherical profiles are then imported into ZEUS-MP.

The four evolutionary stages of the 1.35×10^5 $M_\odot$ primordial halo used in our study are shown in Figure 4. Their central densities range from 1.43 to 1596 cm^{-3}. We consider consecutive profiles from a single halo rather than sampling the entire cluster at a fixed redshift for three reasons. First, the halos in the cluster have similar profiles and are largely coeval, so the emergent I-front may encounter a narrower range of density gradients at a single redshift than in one halo over a range of redshifts. Second, the time at which the cluster is engulfed by the expanding H II region is an open parameter. Finally, we avoid constraining our results to a single cluster of halos and its associated properties (number of peaks, radius, etc.). The possibilities for radiative feedback in the entire cluster are better explored by evaporating a single halo whose central densities vary from low values that are easily ionized to high values in which core collapse would proceed uninterrupted.

This halo mass was selected because it is the smallest in which a star would be expected to form. The I-front would have less impact on more massive halos, so feedback effects would be most prominent in this one. This is roughly twice the minimum halo mass chosen by AS07, who adopted the smallest halo capable of collapsing to core densities of 10^8 cm^{-3} (which marks the onset of three-body H_2 production and runaway cooling) in a Hubble time. A more self-consistent choice would be the minimum halo mass that could reach these densities before being disrupted by mergers, ~20 Myr at $z \sim 20$.

Each profile was illuminated by a 120 $M_\odot$ star at four distances: 150, 250, 500, and 1000 pc. This star's blackbody spectrum is representative of those in the 100–500 $M_\odot$ mass range. These distances exceed the actual range of separations between star and satellite in the chosen Enzo simulation (200–500 pc) but are typical of the other clusters formed in the O'Shea & Norman (2007) survey. Feedback from lower mass Population III stars (30–80 $M_\odot$) warrant separate study because their spectra are not as hard as those of very massive stars and may drive different chemistry in the halos. They also illuminate them for longer times (but not for merger times that would require dark matter dynamics in the simulations). We tabulate our grid of models in Table 1.

We employ the same computational box, resolution, and boundary conditions used in § 2. The halos are again set in hydrostatic equilibrium by computing the gravitational potential necessary to cancel pressure forces in the gas. As before, this potential is held constant over the entire simulation while the self-gravity of the gas is evolved throughout. The halos do exhibit infall velocities as shown in Figure 4, but they are relatively mild. Their inclusion would only slightly aid positive feedback effects and be irrelevant to negative feedback or the destruction of the halo.

For simplicity, we assume ionization and H_2 fractions of 1.0×10^{-4} and 2×10^{-6}, respectively, appropriate for the IGM at $z \sim 20$. Free electron fractions can be depressed below this value in the cores of denser halos by recombinations. This can lead to minor errors in equilibrium H_2 fractions if the halo is photodissociated because they are set by the balance between destruction by LW flux and production by the H^- channel. Uniform ionization fractions can lead to overestimates of H^- in the core, but H_2 fractions are so low when the halo is dissociated that cooling is effectively halted there anyway. Recombinations in the core soon reduce free electron fractions to levels approximating those in the Enzo models, mitigating initial overestimates.

We somewhat underestimate cooling in the core in the course of photoevaporation by imposing uniform H_2 fractions, but this too results only in minor inaccuracies. Diffuse halos are dissociated by LW flux (and would condense very little in 5 Myr without the star). The free electron fractions very rapidly establish H_2 concentrations approximating those in the Enzo halos in denser halos shielded from LW photons, so cooling proceeds nearly uninterrupted. Initial H_2 fractions in halos of intermediate densities that are only partially dissociated are reset to the equilibrium established by production through the H^- reaction and destruction by

TABLE 1
HALO PHOTOEVAPORATION MODELS

n_c (cm^{-3})	150 pc	250 pc	500 pc	1000 pc
1.43	023_150pc	023_250pc	023_500pc	023_1000pc
10.5	039_150pc	039_250pc	039_500pc	039_1000pc
108	059_150pc	059_250pc	059_500pc	059_1000pc
1596	073_150pc	073_250pc	073_500pc	073_1000pc

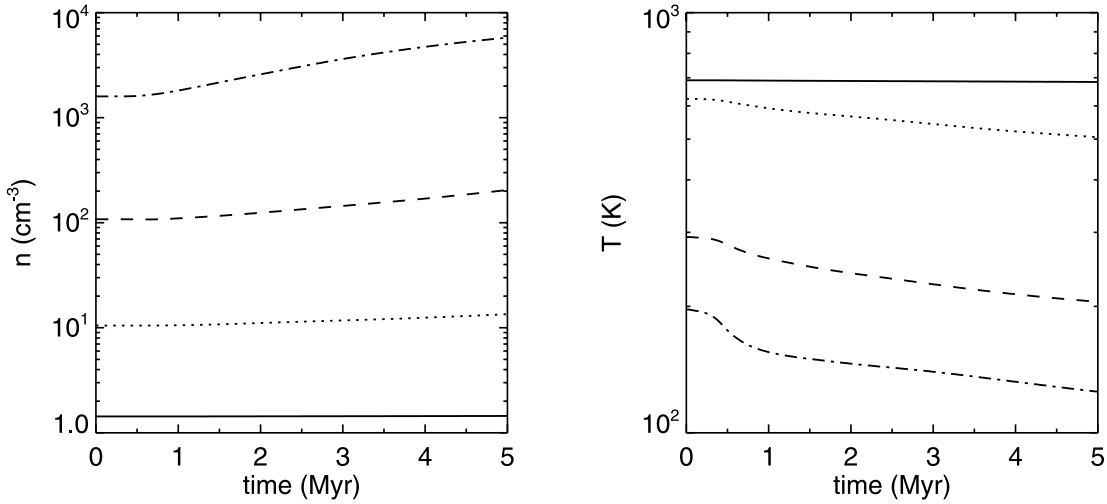

FIG. 5.—Central densities and temperatures over 5 Myr in the absence of external radiation. *Solid lines*: 023 halo; *dotted lines*: 039 halo; *dashed lines*: 059 halo; *dot-dashed lines*: 073 halo.

LW photons. H_2 cooling is not very prominent in such halos and is halted if core H_2 fractions fall below 1×10^{-4}.

In Figure 5 we show the evolution of central densities and temperatures in all four halo profiles over 5 Myr, including Enzo H_2 fractions, the uniform ionization fraction, and no radiation. H_2 cooling causes little changes in the 023 and 039 halos because cooling rates are small in their diffuse cores. Both free-fall and cooling times are much shorter in the denser profiles: central densities in the 059 core rise from 108 to 200 cm^{-3}, and from 1600 to 5000 cm^{-3} in the 073 halo. Photodissociation is unlikely to delay collapse in the first two halos because they evolve little even in the absence of LW flux. H_2 in the cores of the denser halos will likely be shielded in some cases, allowing densities to continue to rise even as the front evaporates them. The evolution timescales of these profiles are consistent with free-fall times $t_{\rm ff} = (3\pi/32G\rho)^{1/2}$ at the halo centers, which vary from 1.17 to 38.2 Myr. Significant contraction would be expected in the densest structure over 5 Myr, while very little would be expected to occur in the most diffuse halo, as corroborated by our findings.

4. RESULTS

We find four outcomes for the halos: (1) undisturbed cores; (2) complete disruption by an R-type or D-type front; (3) perturbed cores, probably with accelerated star formation; and (4) a deformed core partially exposed to the IGM and eroded over time by ionized outflows. The photoionization of the TIS halo described in § 2 serves as a rough template for these models.

4.1. *Undisturbed Cores*

Relatively dense halos are marginally ionized by the central star, and the shock driven by the I-front into the cloud mostly dissipates before reaching the core. Molecular hydrogen in the cores of these halos is shielded from the LW flux of the star, even without the H_2 formed in the front. Core collapse thus continues as the front ionizes the outer layers of the halo. In Figure 6 we show profiles of ionized fraction, density, temperature, pressure, H_2 fraction, and velocity along the z-axis at three stages of photoevaporation in the 073_500pc run, with $n_c = 1596$ cm^{-3} and the star 500 pc from the center of the halo. At 200 kyr the I-front is still R-type (it becomes D-type 50 pc from the center of the cloud). LW photons passing through the front partially dissociate the outer halo, but the core remains deeply shielded and molecular hydrogen levels rise rapidly there. Figure 8*a* shows that the core blocks LW photons in a ~10 pc band centered on the z-axis. Central molecular hydrogen fractions rise from 2×10^{-6} to 1×10^{-4} before the front becomes D-type, leveling off thereafter for the lifetime of the star. H_2 fractions in the R-type front climb to 2×10^{-4} and remain steady after the front transforms to D-type.

The D-type front again has a cometary appearance, but axial compression of the shadow is much slower due to the greater densities in the outer regions of the cloud. The cylindrical shock never reaches the axis in this run. Perturbations are present in the front above the axis at 800 kyr. These fluctuations may be an early stage of instability that arises in D-type fronts in which UV photons are oblique to the shock (Williams 2002). The perturbations are longer farther from the central axis where radiation is incident to the front at smaller angles. LW photons preferentially stream through the underdensities, dissociating H_2 beyond in bands visible between $z = 50$ and $z = 100$ pc at 2.29 Myr in Figure 8*b*. These features are transient, vanishing by the time the star dies. The shock decelerates from 10 km s^{-1} at 50 pc to 7.5 km s^{-1} 25 pc from the core at 2.5 Myr.

When recombination commences at 2.5 Myr molecular hydrogen forms most rapidly in the shock but then radiates outward down the density gradient in the ionized regions of the halo, as shown at 2.59 Myr in Figure 8*c*. H_2 fractions rise more gradually in the core over the following 2.4 Myr, by approximately 50%. The 5.0 Myr curves in Figure 6 show that the center of the cloud is impervious to recombination flows: the incoming shock (eventually approaching to within a few parsecs), the rarefaction wave, ionized backflows at larger radii, and the compression of the shadow toward the axis. Perhaps the most interesting feature of the relic H II region is the appearance of Rayleigh-Taylor instabilities at the interface of the warm ionized gas and shock remnant in Figures 7*b* and 7*d*. The fingers of partially ionized (and rapidly cooling) gas lengthen along the arc away from the axis, but do not affect the dynamics of the core.

Cooling continues in the center of the halo throughout the simulation, with core temperatures falling from 200 to 100 K and densities rising from 1596 to ~3000 cm^{-3} over 5 Myr. The shock remnant eventually ripples through the center but with only minor density fluctuations. Radiation does not deter star formation in this model. The evolution of the halo 1000 pc from the star is basically the same, and radiation does not interrupt the collapse of the core.

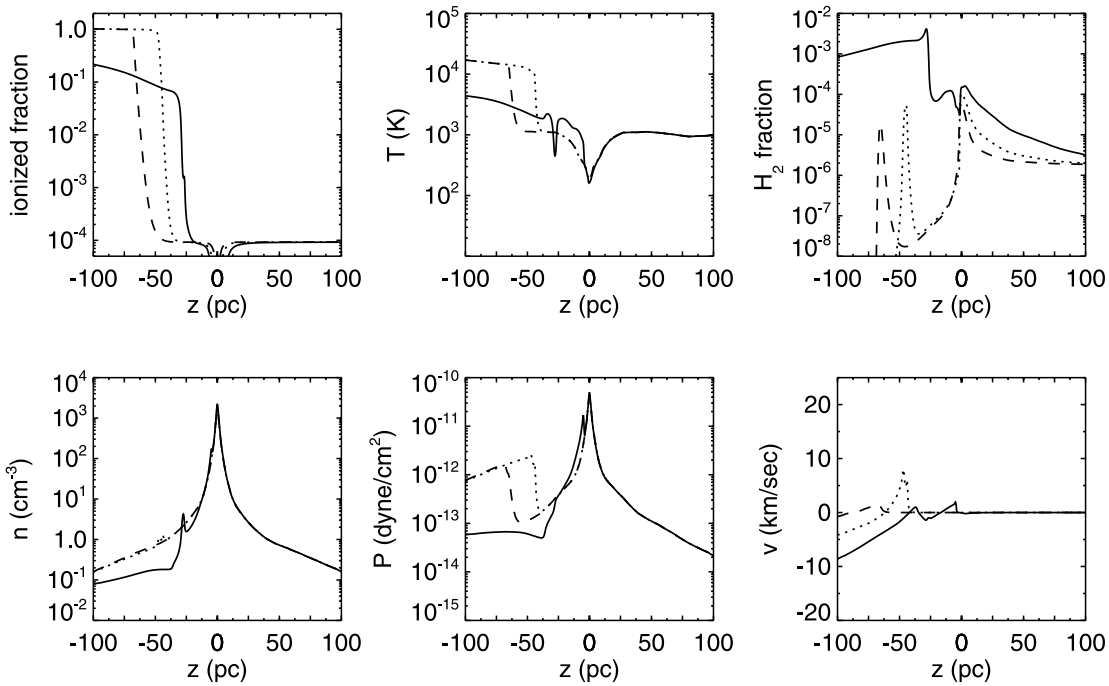

FIG. 6.—Ionized fraction, density, temperature, pressure, H_2 fraction, and velocity profiles for the 073_500pc model. *Dashed lines*: 200 kyr (the R-type front); *dotted lines*: 800 kyr (the D-type front); *solid lines*: 5.0 Myr (the relic H II region).

We find in both cases that the core continues to contract while the front photoionizes the halo, reaching final densities similar to those when no star is present (see Fig. 5).

4.2. *Complete Core Disruption*

In the other extreme, diffuse halos are easily destroyed by the radiation of the star wherever they reside in the cluster, either by an R-type front that ionizes the cloud on timescales much shorter than its dynamical time or by a D-type front that snowplows gas from the core at speeds greater than its escape velocity. We show in Figure 9 the evaporation of the 023 halo ($n_c = 1.43$ cm^{-3}) along the z-axis 500 pc from the star. The star photodissociates the cloud well before the front reaches it, and the equilibrium H_2 fractions drop to less than 1% of their original value. Molecular hydrogen fractions in the front rise over time, from 2×10^{-5} at 225 kyr to 2×10^{-3} at 2.5 Myr. However, the relatively low

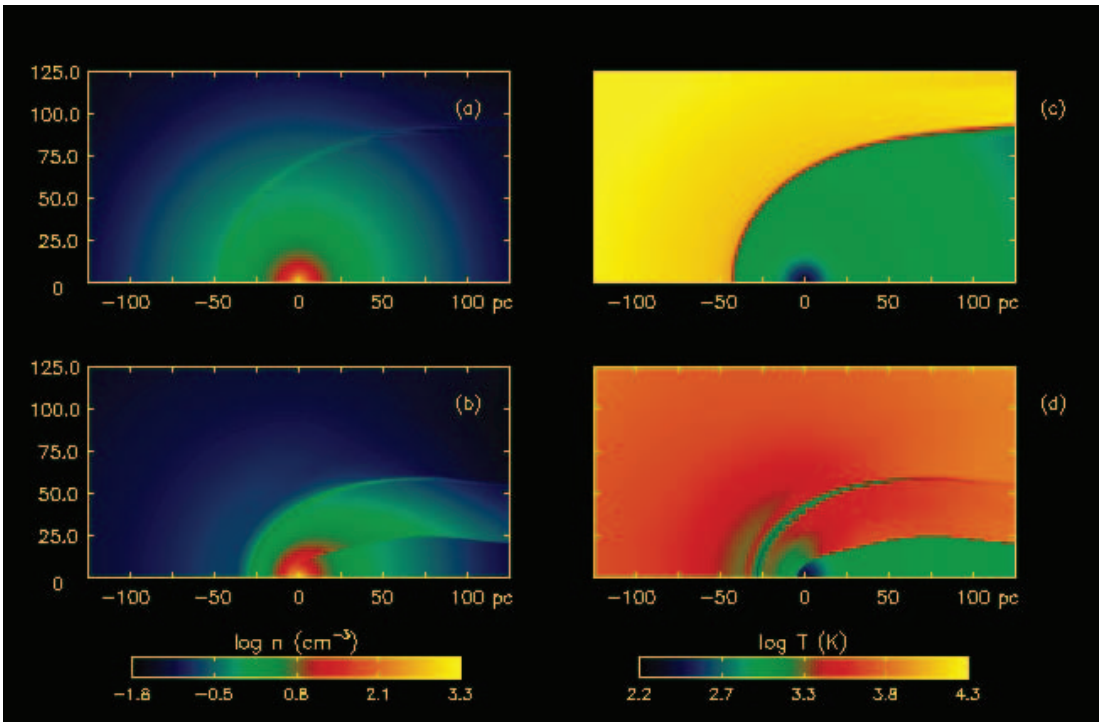

FIG. 7.—Halo evaporation: model 073_500pc. Panels (*a*) and (*b*) are densities at 800 kyr and 5.0 Myr, respectively. Panels (*c*) and (*d*) are temperatures at 800 kyr and 5.0 Myr, respectively.

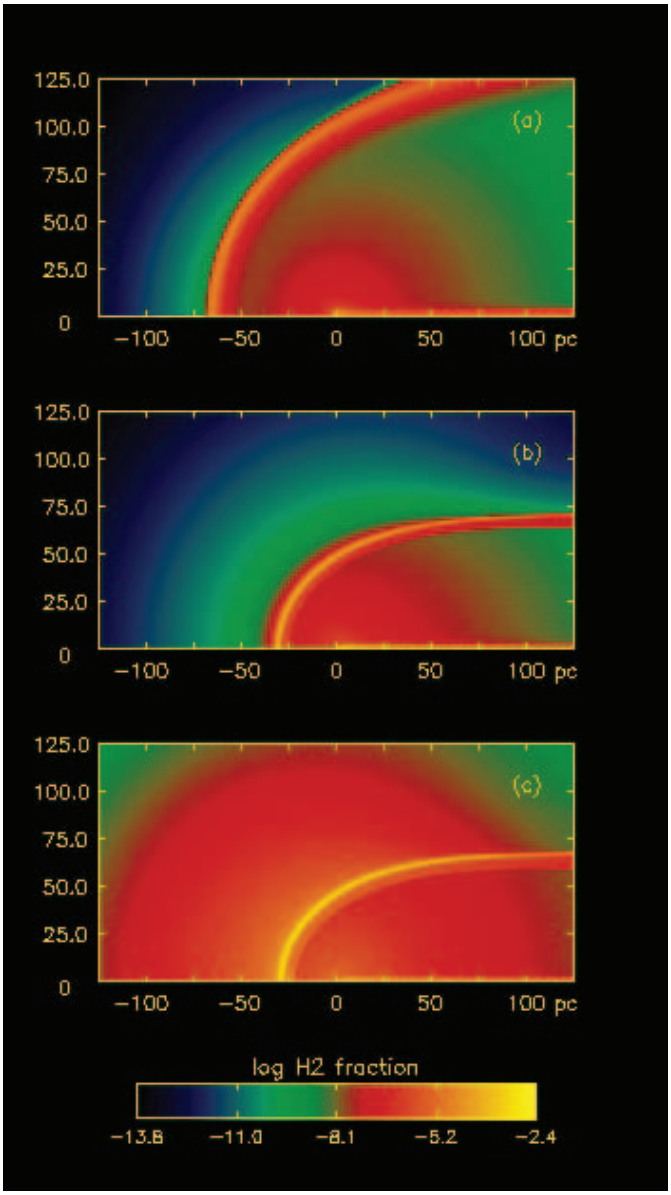

FIG. 8.—H_2 fractions: model 073_500pc. Panels (*a*), (*b*), and (*c*) are at 210 kyr, 2.29 Myr, and 2.59 Myr, respectively.

densities in this halo profile cannot produce sufficient H_2 to shield the core, so its levels remain too small to provide significant cooling. The R-type front executes a transition to D-type ∼15 pc from the core. The halo casts a narrow shadow (Figs. 10*a* and 10*c*) that is crushed into the *z*-axis before the death of the star. The shock heats to over 15,000 K, inciting rapid molecular hydrogen catalysis along several segments of the axis at once by collisional ionization as shown in the 2.5 Myr ionization, H_2, and temperature profiles in Figure 9.

Before the star dies the shock focuses the core into a compact fragment whose densities at 2.5 Myr exceed 400 cm^{-3}. The shock drives this clump 25 pc from the center of the halo by 2.5 Myr at velocities of 10–20 km s^{-1}. As gas recombines it recedes from both the fragment and the axis in spherical and cylindrical contours evident in Figures 10*b* and 10*d*. The fragment remains fairly stable along the axis but expands somewhat over time, as shown in the 5.0 Myr density profile. The front of the clump is shocked gas at 1000–1500 K, but it quickly cools to a few hundred kelvins due to H_2 fractions of 5×10^{-4} to 1×10^{-3}.

Can the clump fragment into a star? At the fragment's average density and temperature of 3 cm^{-3} and 150 K, its Jeans mass,

$$m_{\rm J} = \left(\frac{5k_{\rm B}T}{G\mu m_{\rm H}}\right)^{3/2}\left(\frac{3}{4\pi\rho_{\rm cl}}\right)^{1/2}, \qquad (5)$$

is 7.4×10^4 $M_\odot$, far greater than the ∼20 $M_\odot$ in the clump. This together with its expansion from 300 to 3 cm^{-3} over 2.4 Myr preclude its collapse into a star.

The 023 halo is destroyed at all four distances from the star. When it is only 150 pc away it is flash ionized by an R-type front in 200 kyr. Pressure gradients in the now ionized but otherwise undisturbed density profile drive strong outflows that evict all the gas from the halo within 3 Myr at speeds far above the escape velocity. These gradients persist until the original density profile is paved nearly flat: 4×10^{-2} cm^{-3} at 5 Myr. The relic H II region uniformly cools to only 6000 K and ionized fractions of 50% at 5 Myr because recombinations are so strongly suppressed in the diffuse gas. Molecular hydrogen is collisionally dissociated to extremely low levels by the R-type front, but reforms soon after the death of the star. Final H_2 fractions mirror the densities at the end of the run and are roughly level at 1×10^{-4}.

The I-front becomes D-type at $z = 0$ pc, the very center of the halo, at 220 kyr when the halo is 250 pc from the star. As at 500 pc, the cloud is first strongly dissociated by LW flux and the I-front shock again forges a small, cool, dense fragment on the axis that survives to 5 Myr, but it is less massive and more turbulent. With densities <1 cm^{-3}, the fragment is swept from the halo by the shock at speeds of 5–7 km s^{-1}. These lower ejection velocities are governed by the I-front driving the shock rather than the stronger pressure gradients of the fully ionized isothermal halo in the 023_150pc model. When the halo is 1000 pc from the star the front becomes D-type 25 pc from the core, which is dissociated to H_2 fractions of 1×10^{-7}. A denser clump is formed than in the 023_500pc model, but its mass again falls far short of the Jeans mass. We note that strong rarefaction waves form and evacuate gas exterior to the clump from the halo; they are visible as the green circular arc in Figure 10*b*. They are in all 023 runs in which the front becomes D-type. As a rule, complete collisional or LW dissociation of the halo occurs whenever the core is totally disrupted by the front.

The evolution of the 039 halo 150 and 250 pc from the star closely resembles that of the 023_250pc, 023_500pc, and 023_1000pc models. The fragment formed in the 039_250pc run was 2300 $M_\odot$, the most massive encountered in the completely disrupted halos. This mass approaches the Jeans mass for the density of the clump (∼400 cm^{-3}), raising the interesting possibility of cloud fragmentation into a new star in slightly denser halos illuminated at somewhat greater distances. Had HD cooling been included in this model, the temperature of the fragment might have fallen to the CMB temperature, ∼50 K at the redshifts of these halo profiles, reducing its Jeans mass by a factor of 5 and ensuring its breakup. Nevertheless, we conclude that radiation feedback on star formation in this sector of the flux-n_c plane is overwhelmingly negative. Compression of the halo into a dense fragment will be a general feature of diffuse halo evaporation because of the rapid destruction of their shadows, even in three dimensions. Halos evolved from cosmological initial conditions exhibit roughly spherical morphologies that may cause similar focusing.

4.3. *Accelerated Collapse*

Within a band of fluxes and central densities, the I-front can jostle the core of the halo with a shock enriched with H_2, compressing and speeding its collapse without destroying it. We show

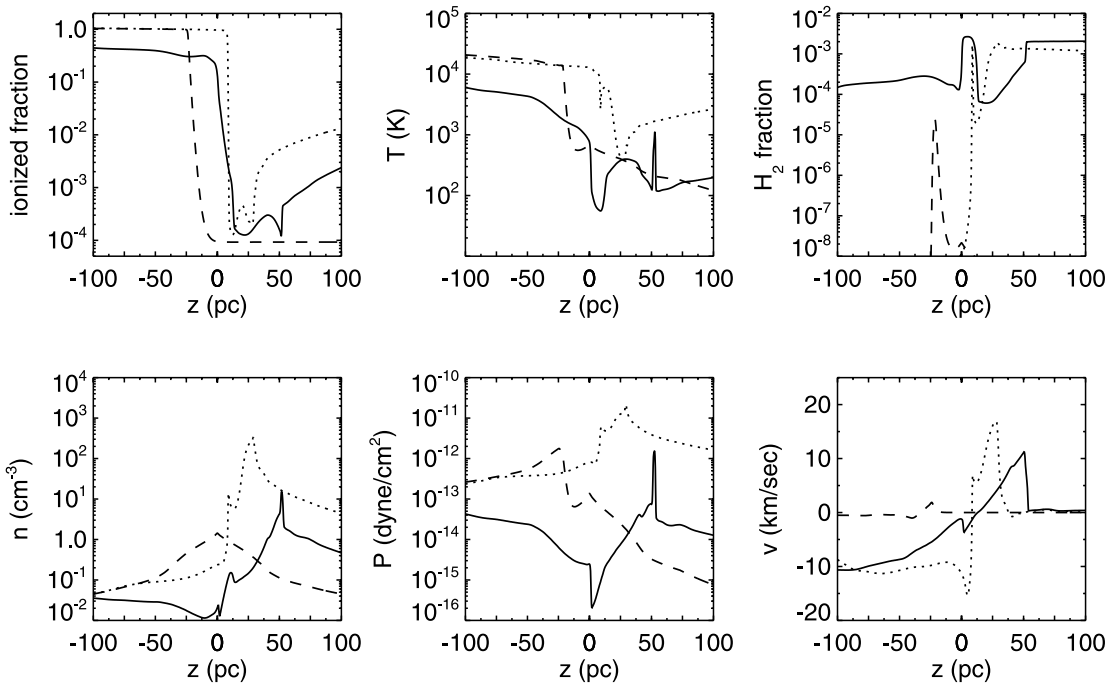

FIG. 9.—Ionized fraction, density, temperature, pressure, H_2 fraction, and velocity profiles for the 023_500pc model. *Dashed lines*: 225 kyr (the R-type front); *dotted lines*: 2.5 Myr (the D-type front); *solid lines*: 5.0 Myr (the relic H II region).

in Figure 11 flow profiles along the central axis for the 039 halo ($n_c = 10.5$ cm^{-3}) 500 pc from the Population III star. The star initially photodissociates the cloud, leaving only 5% of the original H_2 in the core at 225 kyr. The front converts to D-type 40 pc from the center and is 15 pc away when the star dies. The velocity of the front is 10 km s^{-1} at 2.4 Myr in Figure 11 (having been constant from -40 to -15 pc) but is less than 2.5 km s^{-1} on reaching the core at 5.0 Myr. Gas just beyond the core is shot forward as the halo shadow squeezes the *z*-axis, but the gas in the core continues to slow. The density at the center of the cloud is 30 cm^{-3}, and its molecular hydrogen fraction is 2×10^{-4} at 5.0 Myr.

The gas launched forward from the halo by axial implosion is at speeds well above the escape velocity and cannot contribute to star formation in the core. This jet would not be as focused in a three-dimensional simulation with an actual halo, but it would still tend to eject matter from the far side. The core is somewhat displaced from the center of the halo but remains there in spite of

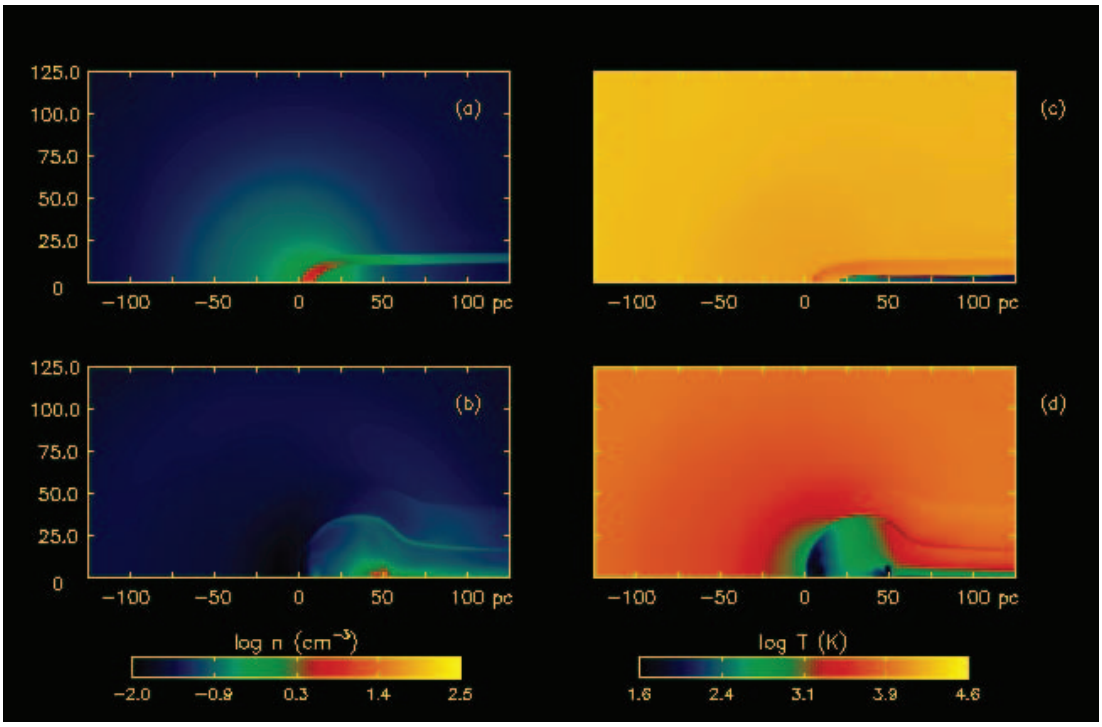

FIG. 10.—Halo evaporation: model 023_500pc. Panels (*a*) and (*b*) are densities at 1.69 and 5.0 Myr, respectively. Panels (*c*) and (*d*) are temperatures at 2.02 and 5.0 Myr, respectively.

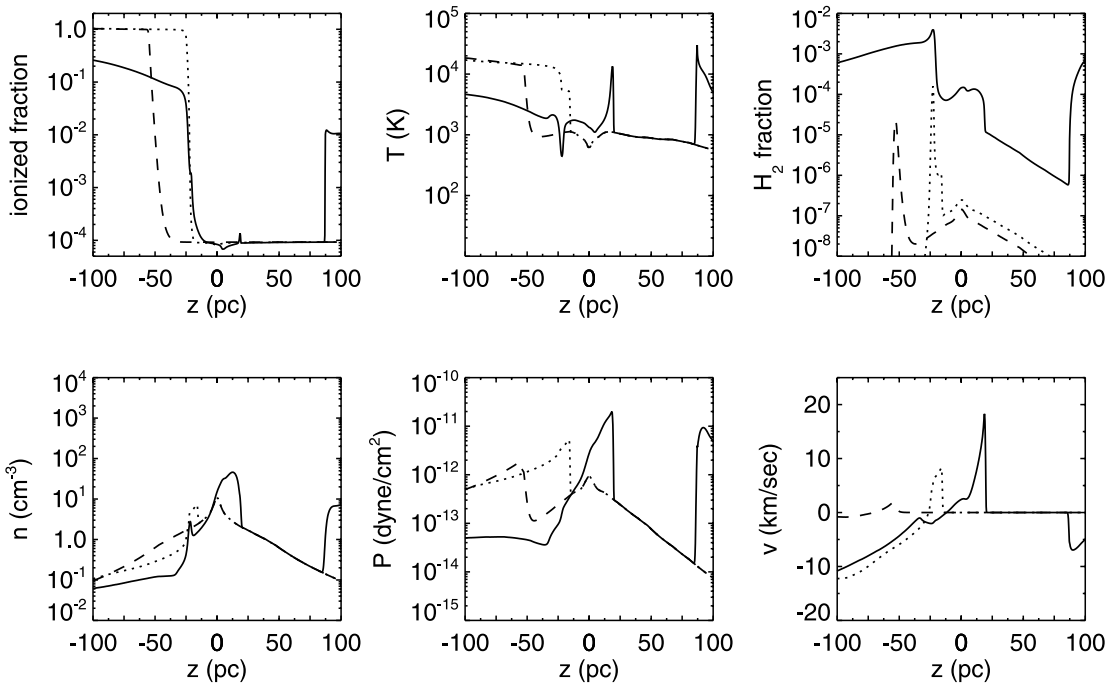

FIG. 11.—Ionized fraction, density, temperature, pressure, H_2 fraction, and velocity profiles for the 039_500pc model. *Dashed lines*: 225 kyr (the R-type front); *dotted lines*: 2.4 Myr (the D-type front); *solid lines*: 5.0 Myr (the relic H II region).

the jet. With final densities nearly 3 times what would have been present at 5 Myr in the absence of radiation, star formation is probably accelerated in this core. However, to capture the true timescales on which the 1000 K core cools and collapses into a star, we must follow its displacement from the center of the halo with high-resolution AMR calculations currently under development.

The density and temperature panels in Figure 12 reveal two interesting features. First, a strong rarefaction wave again detaches from the rear of the halo in the recombinational flow, rapidly cooling as it grows. At 5 Myr the wave has withdrawn to $z = -25$ pc, with a density of 2–3 cm^{-3} and temperature of $\sim$300 K. Second, the shadow strikes the z-axis at two positions at once, $z = 15$ and $z = 75$ pc. The implosion rebounds from the axis beyond 75 pc, again creating molecular hydrogen by collisional ionizations.

Feedback in the 039 halo 1000 pc from the star will be more conclusively positive because the remnant slows even more before reaching the core. Initial dissociation of the core is not as severe at this distance, with a H_2 equilibrium value that rises to 2×10^{-6} by 2.5 Myr. The shock in the relic H II region is over 13 pc from the core at 5.0 Myr with a rarefaction wave at -40 pc. The core of the 073 halo 250 pc from the star is also density enhanced but follows a different evolutionary path. The shock reaches the core at 3.75 Myr at velocities less than 1 km s^{-1}, raising its density from 1600 to 5000 cm^{-3} at a temperature and H_2 fraction of 175 K and 2×10^{-5}, respectively. Collapse of the core would be strongly accelerated in this instance, but the cylindrical implosion behind the halo drives gas back into it from the right, somewhat reducing the density of the core. Neglecting backwash from the shadow, which would be significantly weaker in three dimensions, we conclude that radiation exerts positive feedback on star formation in this model. The halos in the 059_500pc and 059_1000pc runs follow similar evolutionary tracks, but in these cases the shadow is still far from the z-axis at 5 Myr, so backflows do not reach the core.

Interestingly, I-front instabilities similar to those in the 073_500pc model develop in the 073 halo 250 pc from the star at 400 kyr. In this case the unstable modes become completely nonlinear away from the axis, extending long fingers of ionized gas nearly parallel to the arc forward into the neutral gas. However, these fingers are crushed downward toward the axis as the shadow narrows, creating colliding shock fronts that roil gas in the otherwise smooth arc. The perturbations grow much larger because they form sooner than in the 073_500pc model. However, as before, they have no impact on the core. This halo is partially dissociated, in the sense that equilibrium H_2 values are somewhat depressed below the levels present at 500 and 1000 pc. Core molecular hydrogen abundances fall below 1×10^{-4}, so the halo ceases to condense while being ionized.

We show in Figure 13 flow profiles for the 059_150 pc model at 50 kyr, 2.5 Myr, and 5.0 Myr. The core is at first dissociated to low molecular hydrogen fractions ($\sim 6 \times 10^{-8}$) by the star. The I-front forms a shock 20 pc from the halo; as it ascends the density gradient toward the center, its density rivals that of the core just before merging with it at 2.0 Myr. The shock becomes nearly opaque to LW flux from the star, and H_2 catalysis shoots rapidly upward to 2×10^{-4} from 1 to 2.5 Myr, effectively reversing the initial photodissociation. As the shock merges with the core its density climbs from 108 to 500 cm^{-3} at 2.5 Myr. At nearly the same time the core is closed off from the right as collapse of the halo shadow meets the z-axis, as shown in Figures 14*a* and 14*c*. The coordinated flows drive central densities to 2000 cm^{-3}, mostly halting their displacement to the right. At 5 Myr the core is nudged 5 pc from the origin but at velocities of less than 2 km s^{-1}. The density of the core diminishes to 700 cm^{-3}, mostly due to eddies above the origin evident in Figures 14*b* and 14*d*. The center of the cloud remains fairly compact and falls to temperatures of $\sim$100 K. Velocities are nearly flat from 0 to 50 pc at 5 Myr. Of all the models, collapse of the core into a star would be amplified most in this one. In this instance backflow from the shadow into the core reinforces rather than delays collapse; even though our

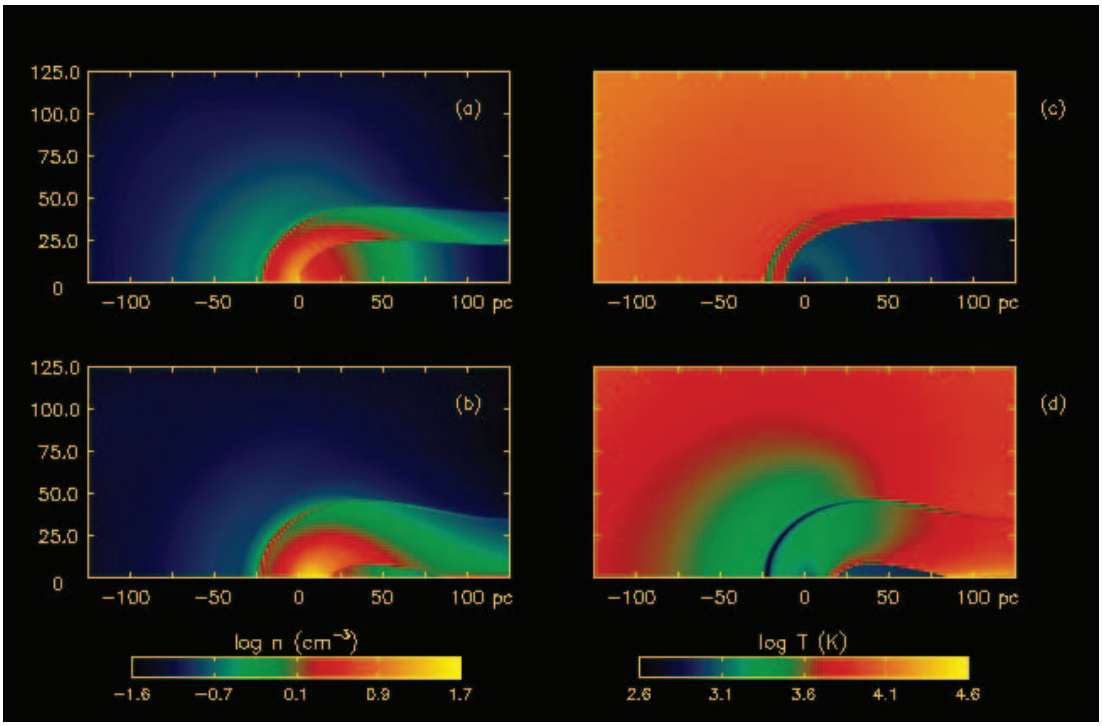

FIG. 12.—Halo evaporation: model 039_500pc. Panels (*a*) and (*b*) are densities at 3.65 and 5.0 Myr, respectively. Panels (*c*) and (*d*) are temperatures at 2.75 and 5.0 Myr, respectively.

idealized two-dimensional geometry overestimates this flow, it would still be present in three-dimensional models. Collapse would likely be enhanced, albeit somewhat off-center in the dark matter halo.

4.4. *Drained Cores*

In a less forgiving sector of the flux-n_c plane the shock remnant displaces the core more violently and the implosion of the shadow deforms it more severely, but it still survives. In these cases the core tends to spring back from compression and be eroded by the rarefaction wave and relic ionized outflows. Central densities fall rapidly in the wake of the shock on dynamical timescales that may be shorter than cooling and collapse times. Figure 15 shows flow curves through the center of halo 059, 250 pc from the star, and Figure 16 shows density and temperature images of the evaporating halo. The star dissociates the halo, reducing H_2

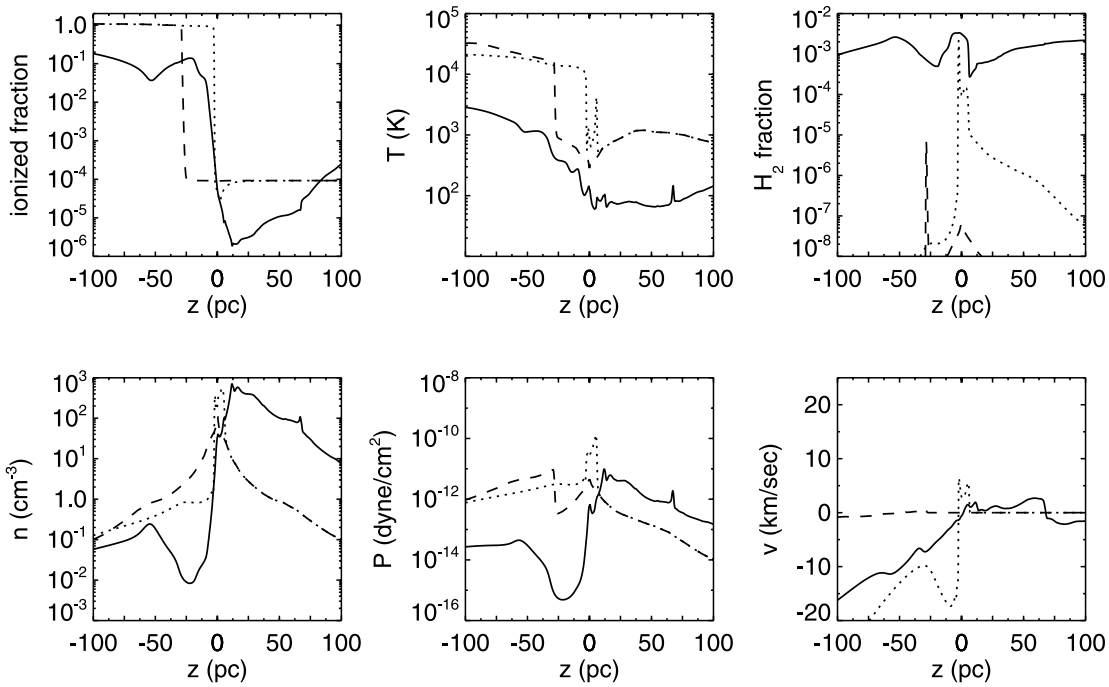

FIG. 13.—Ionized fraction, density, temperature, pressure, H_2 fraction, and velocity profiles for the 059_150pc model. *Dashed lines*: 50 kyr (the R-type front); *dotted lines*: 2.5 Myr (the D-type front); *solid lines*: 5.0 Myr (the relic H II region).

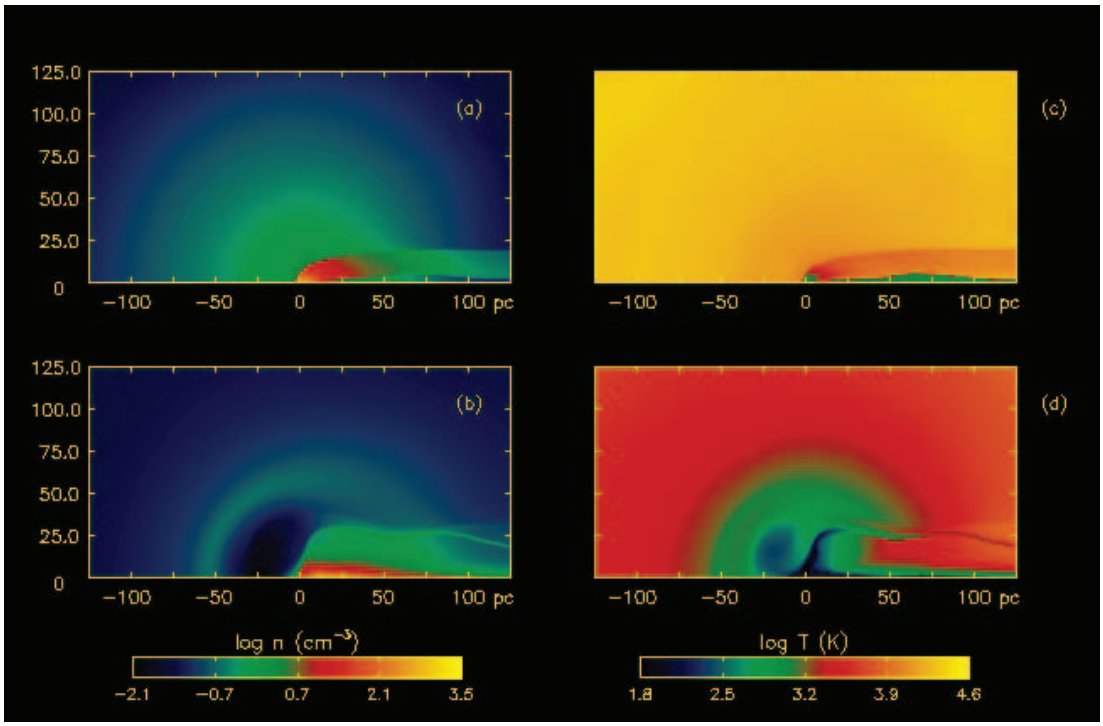

FIG. 14.—Halo evaporation: model 059_150pc. Panels (*a*) and (*b*) are densities at 2.5 and 5.0 Myr, respectively. Panels (*c*) and (*d*) are temperatures at 2.5 and 5.0 Myr, respectively.

fractions at the center to a tenth of their original value by 225 kyr. The I-front becomes D-type 32 pc from the core. Unlike the 059_150pc run, the front never allows molecular hydrogen to reform at the center because at 2.5 Myr it is still 7 pc from the origin, not close enough to snowplow H_2-enriched gas into a shield capable of protecting the core from the LW photons.

The shock reaches the center of the cloud at 3.5 Myr, boosting its density from 108 to 300 cm^{-3}. The 3 km s^{-1} remnant collides with a backflow shock from the collapsing shadow shortly thereafter, driving the displaced core briefly to densities of 800 cm^{-3} at 4.5 Myr. This gas is moving at nearly the escape speed, but will likely decelerate as it advances to the right. However, at $z = 0$ the gas is at 200 cm^{-3} and moving at sub–km s^{-1} speeds. Since it is still centered in the dark matter potential, one might expect its collapse to accelerate, but its density continues to rapidly fall because of the steep velocity gradient to the left of $z = 0$ established when the front ablates the halo. Hence, even though the core is compressed it is also smeared along the z-axis by both the remnant

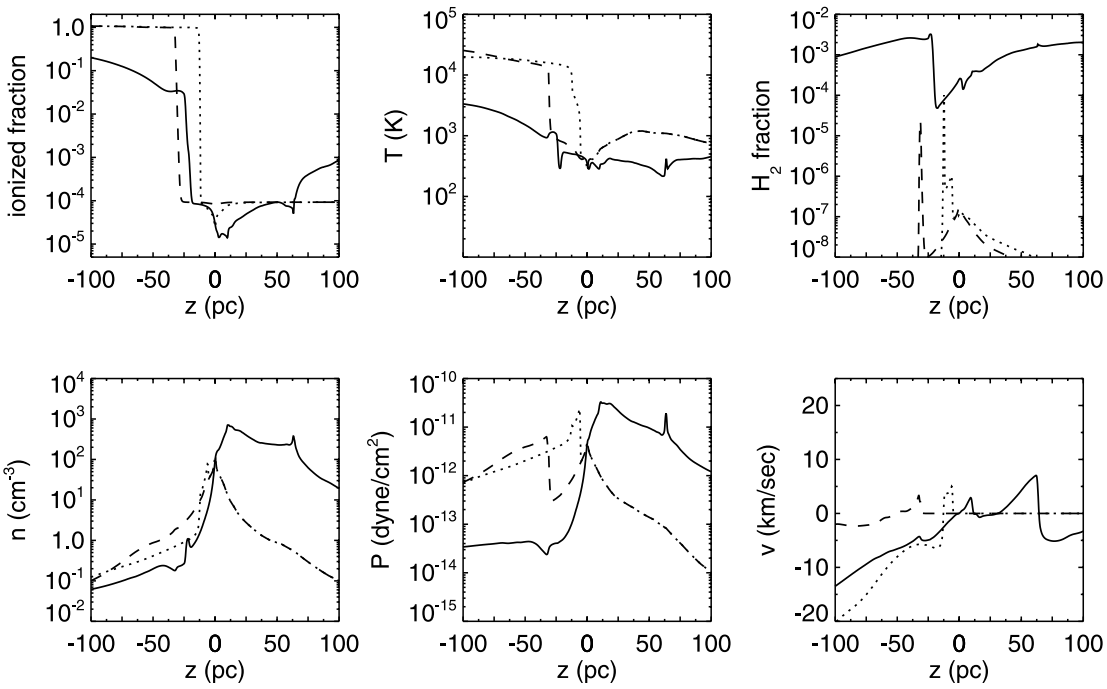

FIG. 15.—Ionized fraction, density, temperature, pressure, H_2 fraction, and velocity profiles for the 059_250pc model. *Dashed lines*: 225 kyr (the R-type front); *dotted lines*: 2.4 Myr (the D-type front); *solid lines*: 5.0 Myr (the relic H II region).

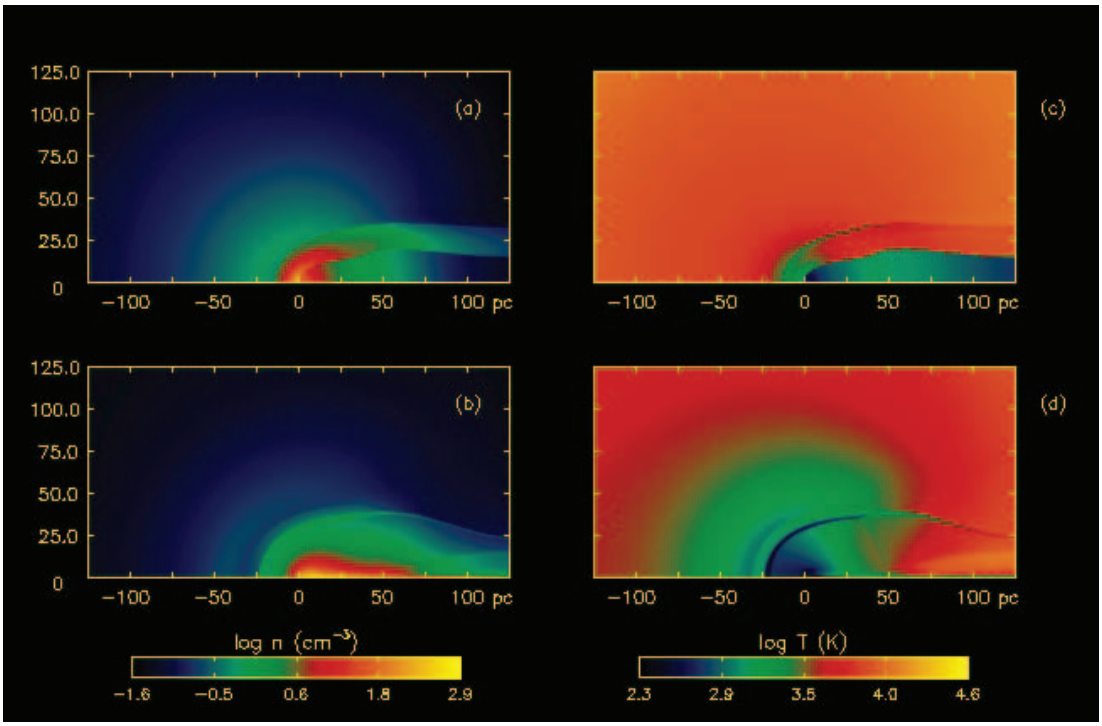

FIG. 16.—Halo evaporation: model 059_250pc. Panels (*a*) and (*b*) are densities at 3.03 and 5.0 Myr, respectively. Panels (*c*) and (*d*) are temperatures at 3.03 and 5.0 Myr, respectively.

and the axial shock. We cannot state the ultimate fate of the core with certainty in these circumstances and reserve it for further study. The evolution of the 073 halo illuminated from 150 pc is very similar to that of the 059_250pc model. The main difference is that the D-type front comes close enough to the core for its shock to completely shield it from LW flux, as in the 059_150pc model.

We tabulate the effect of UV radiation on star formation in each model and the degree of dissociation of the halo prior to the death of the star in Figure 17. A clear trend in feedback ranging from neutral to positive to negative is evident in dense halos illuminated at large distances to diffuse halos close to the star. The two question marks refer to deformed cores in which collapse is uncertain. The D, R entry in the dissociation table signifies that H_2 in the core is initially destroyed by the star but then allowed to reform due to shielding by the front. The two D, E entries are similar, except that the core H_2 levels surpass their original values before the death of the star. S, E means that the original core molecular hydrogen is self-shielded from LW flux and then rises during the life of the star. A trend in dissociation is apparent: massive cores far from the star retain their H_2, while lighter cores close to the star do not.

4.5. *Recombination Radiation*

As observed earlier, in neglecting direct transport of diffuse radiation we do not obtain the exact geometry of the shadow cast

	1000 pc	500 pc	250 pc	150 pc
1.43 cm^{-3}	D	D	D	D
10.5 cm^{-3}	P	P	D	D
108 cm^{-3}	P	P	?	P
1596 cm^{-3}	N	N	P	?

P = positive feedback, D = disrupted, N = neutral

	1000 pc	500 pc	250 pc	150 pc
1.43 cm^{-3}	D	D	D	D
10.5 cm^{-3}	D,R	D	D	D
108 cm^{-3}	S,E	P	D	D,E
1596 cm^{-3}	S	S	P	D

D = dissociated, P = partly dissociated, S = shielded
E = enhanced, R = restored

FIG. 17.—Radiative feedback on star formation (*left*) and dissociation of the core of the halo (*right*) in each of the photoevaporation models. The ionizing photon fluxes at 150, 250, 500, and 1000 pc are 5.173×10^7, 1.862×10^7, 4.655×10^6, and 1.164×10^7 cm^{-2} s^{-1}, respectively.

by the halo. Reprocessed radiation from the ionized gas bounding the shadow would further degrade it. However, recombination photons above the ionization limit and in the LW band could also alter the timescales of H_2 formation in the relic H II region. This effect would be transient, with the recombination luminosity greatest in the dense ionized gas at the base of the D-type shock. A rough estimate of its impact on H_2 formation can be made by comparison of the recombination flux and the original stellar UV flux. The number density of all recombination photons emitted per unit time is

$$n_{\rm rec} = n_e n_p \alpha_A(T), \tag{6}$$

and the recombination timescale $t_{\rm rec} = n_p/(dn_p/dt)$,

$$t_{\rm rec} = \frac{1}{n_e \alpha_A(T)}, \tag{7}$$

where n_p and n_e are the number densities of protons and electrons, respectively. Taking the 073_250pc model as a fiducial case, at the base of the shock $n_p = n_e \sim 90$ cm^{-3}, and $T \sim 1 \times 10^4$ K. From the recombination rates in Table 1 of Hummer (1994), $T_{\rm rec} \sim$ 850 yr, and the flux of diffuse photons exiting any face of the zone is $\sim 4.3 \times 10^8$ cm^{-3} s^{-1}, which is briefly brighter than the number flux of the star at 250 pc, 1.9×10^7 cm^{-3} s^{-1}. Recombination photons from the shock can outshine the original star, but for less than 1 kyr. This flux would briefly postpone H_2 formation in the vicinity of the remnant but with little final influence on collapse of the core. Recombination times are much longer in the diffuse outer regions of the halo, so its emissivity persists much longer but at far lower luminosities, by factors of 1×10^{-4} to 1×10^{-6}.

5. DISCUSSION AND CONCLUSIONS

Radiation from the 120 $M_\odot$ star permits star formation in moderately evolved halos ($n_c > 2000$ cm^{-3}) at distances greater than 200 pc, but halts it in diffuse halos with central densities below 1–2 cm^{-3} anywhere in the cluster. Since this is likely the least massive halo able to host a star, radiation from the central source would probably prevent star formation in any smaller objects in its vicinity. At intermediate central densities radiative feedback may be positive or negative depending on the flux incident on the halo. In all cases in which the cloud is not destroyed outright, the star dies before the front reaches the core. It is the velocity with which the shock remnant reaches the core of the halo from the left and the extent to which ionized gas in the relic H II region envelops and squeezes the core from above and below that governs whether star formation therein is promoted or suppressed in these two-dimensional simulations. In general, when the geometry of the halo shadow conspires with the ablation remnant to compress the core of the cloud without displacing it too far from the center, star formation is accelerated. Collapse of the center into a star is less certain if the shadow instead crushes the core along the z-axis and it is exposed to strong ionized backflows. In these instances we must resort to detailed AMR calculations to determine the fate of the cloud.

We find in the end that LW radiation from the star exerts little feedback on star formation in the cluster. Diffuse halos are completely ionized, rendering photodissociation irrelevant, while molecular hydrogen in the cores of more evolved structures is deeply shielded from LW flux. Halos of intermediate densities are photodissociated by the star, but H_2 cooling causes little change in these structures over 2.5 Myr, even in the absence of radiation. After the death of the star the H^- channel rapidly restores the dissociated H_2 in the core, with little (if any) delay in its collapse. In some cases the front itself shields the core, permitting H_2 fractions to rise beyond their original values before the death of the star. Halos in which H_2 cooling makes any difference over 5 Myr have much higher central densities than those in this study and would be completely shielded from LW flux.

This is true only of the first few generations of stars before a steady LW background has built up and dissociating photons are present only during the life of the central star. If successive star formation instead proceeds in the cluster or the halos form at later redshifts, they will be illuminated from many lines of sight for greater periods of time. H_2 formation would then be suppressed for longer intervals in larger volumes of the halos than in our study. However, Machacek et al. (2001) have found the effect of this background is to postpone (not prevent) collapse of the baryons in the halo into a star. In this scenario direct LW flux from the star will dominate the background until later redshifts due to the proximity of halos in the cluster. Each satellite would therefore be exposed to both an intermittent and a slowly varying flux. Unless more than one star forms in the cluster the ionizing radiation would always be well represented by a plane wave, since primordial H II regions are limited to radii of no more than a few kiloparsecs, well below the usual separation between clusters. This is generally true of primordial star formation, since the epoch of overlap between cosmological H II regions is at much lower redshifts.

Upgrades to the ZEUS-MP reaction network are in progress to include HD chemistry and cooling, which can play a significant role in the relic H II region wherever significant H_2 fractions form (Johnson et al. 2007; Yoshida et al. 2007). HD in the I-front and halo core can in principle cool the center of the cloud down to the CMB, possibly causing its collapse into a new, less massive primordial star. Primordial star formation may therefore bifurcate directly into a lower mass branch in the second generation, unaided by metals ejected from supernovae. HD cooling may also alter the dynamics of the shock by radiatively cooling it at the expense of its own kinetic energy, delaying its arrival at the core and modifying its final density and structure.

Since we have adopted the least massive halo in which a star can form, our results can be taken as an upper limit for radiative feedback within the cluster because larger halos would be less affected. There is considerable degeneracy in photoevaporation in the flux-n_c plane, so even though more massive stars were not considered in this survey, many of our results would be relevant to brighter sources at greater distances from the halos. Likewise, cores whose survival is nominal in this survey would almost certainly be destroyed by more luminous stars. However, our study should be extended to less massive stars (40–80 $M_\odot$) for two reasons. First, these stars irradiate neighboring halos for longer times, and the I-front shock and implosion of the shadow may coordinate the compression of the core differently than more intense fluxes. Second, the spectra of these stars are softer, modifying the structure and chemistry of the I-front itself. It is unclear whether more or less H_2 is manufactured in these fronts; although fewer hard photons ionize its outer layers, less LW flux dissociates the molecules, raising the question of how much H_2 the shock would deliver to the core.

These results are in general agreement with Susa & Umemura (2006) and Susa (2007), but differ significantly from AS07. First, we find that SIMF plays no role in star formation in cosmological minihalos at high redshifts, because neither the D-type front nor its remnant ever heat the core above a few thousand kelvins. We observe SIMF in the implosion of the shadow, but it never mixes with the center of the cloud, and in any event is an artifact of the

radial symmetry assumed for the halo. We doubt this effect to be important in three-dimensional calculations in which the true morphology of the halos would break the symmetry of the implosion. Furthermore, one-dimensional models fail to capture the shadow of the halo or its deformation of the core, which in some cases is quite serious. That said, we find our results to qualitatively agree well with the two-dimensional halo photoionization models of Shapiro et al. (2004). Although primordial chemistry was not included in those calculations, they exhibit similar shadowing of the I-front, transformation of the I-front from R-type to D-type along the central axis, and morphologies in outflow. Even without H and He chemistry these models much better represent the ionization of cosmological halos than one-dimensional calculations.

However, two-dimensional models suffer from their own limitations, one being that they do not fully reproduce how the relic H II region envelops and compresses the evaporated halo. The ablation remnant from the left together with relic H II surrounding the halo mold the core in concert; shocked flows from the shadow will be less coordinated or symmetric in three dimensions with real halos. Minihalo photoevaporation must be revisited in three dimensions in order to assess the true role of shadow implosion in core dynamics. We also note that our calculations do not address filamentary inflows into the halos, but we do not expect this to be an important limitation. The filaments threading through halos in our AMR simulations typically have overdensities no greater than 50 times the cosmic mean and so are still relatively diffuse in comparison to the halos into which they flow. Such structures might briefly shadow I-fronts engulfing them but would be quickly photoevaporated, with little dynamical effect on the halo. It is safe to assume that any further inflow to the halo would be cut off in such circumstances.

Nevertheless, we maintain that these models yield accurate measures of the penetration of ionizing and LW UV into minihalos at high redshift because the average density gradients they encounter are derived from cosmological initial conditions. Our study unambiguously identifies the nature of the radiative feedback in many cases while singling out those in which star formation is uncertain for further examination in three dimensions. Extraction of a three-dimensional halo from an Enzo simulation for photoevaporation on a Cartesian mesh in ZEUS-MP would yield an accurately processed cloud core at the end of the main-sequence lifetime of the star. Reinsertion of the evaporated halo into Enzo for further evolution with AMR resolution, dark matter and gas dynamics, and primordial chemistry would follow the migration of a displaced core in the dark matter potential of the halo, clarifying whether a star actually forms.

We have excluded several processes that may be important. First, turbulent velocity fields in halos may incite I-front instabilities in the cloud (Mizuta et al. 2005, 2006). Such instabilities could puncture the core and prevent its collapse into a star. Also, in contrast to the steady luminosities assumed in this study, stellar evolution models predict time-dependent fluxes for massive primordial stars that could modulate photoevaporation timescales. Moreover, if the star detonates in a Type II or pair-instability supernova, metal-enriched ejecta may wash over the halo, a scenario recently explored by Cen & Riquelme (2008). The blast could strip the halo by ram pressure or mix it with metals, radically altering its time and mass scales of collapse. Finally, we have assumed that the halo is no longer illuminated after the death of the star, but in reality it could be irradiated by hard X-ray photons from a black hole remnant capable of partially ionizing the gas without heating it to temperatures fatal to H_2 formation.

We thank the anonymous referee, whose constructive comments improved the quality of this paper. D. W. thanks Tom Abel, Kyungjin Ahn, Greg Bryan, and Alex Heger for helpful discussions concerning these simulations. This work was carried out under the auspices of the National Nuclear Security Administration of the US Department of Energy at Los Alamos National Laboratory under contract DE-AC52-06NA25396. The simulations were performed at SDSC and NCSA under NRAC allocation MCA98N020, and at Los Alamos National Laboratory.

REFERENCES

Abel, T., Anninos, P., Zhang, Y., & Norman, M. L. 1997, NewA, 2, 181
Abel, T., Bryan, G. L., & Norman, M. L. 2000, ApJ, 540, 39
———. 2002, Science, 295, 93
Abel, T., Wise, J. H., & Bryan, G. L. 2007, ApJ, 659, L87
Ahn, K., & Shapiro, P. R. 2007, MNRAS, 375, 881 (AS07)
Alvarez, M. A., Bromm, V., & Shapiro, P. R. 2006, ApJ, 639, 621
Anninos, P., Zhang, Y., Abel, T., & Norman, M. L. 1997, NewA, 2, 209
Bertoldi, F. 1989, ApJ, 346, 735
Bertoldi, F., & McKee, C. F. 1990, ApJ, 354, 529
Bromm, V., Coppi, P. S., & Larson, R. B. 1999, ApJ, 527, L5
Cen, R. 2001, ApJ, 560, 592
Cen, R., & Riquelme, M. A. 2008, ApJ, 674, 644
Ciardi, B., Ferrara, A., & White, S. D. M. 2003, MNRAS, 344, L7
Draine, B. T., & Bertoldi, F. 1996, ApJ, 468, 269
Galli, D., & Palla, F. 1998, A&A, 335, 403
Hayes, J. C., Norman, M. L., Fiedler, R. A., Bordner, J. O., Li, P. S., Clark, S. E., ud-Doula, A., & Mac Low, M.-M. 2006, ApJS, 165, 188
Heger, A., Fryer, C. L., Woosley, S. E., Langer, N., & Hartmann, D. H. 2003, ApJ, 591, 288
Hummer, D. G. 1994, MNRAS, 268, 109
Johnson, J. L., Greif, T. H., & Bromm, V. 2007, ApJ, 665, 85
Kitayama, T., Yoshida, N., Susa, H., & Umemura, M. 2004, ApJ, 613, 631
Kuhlen, M., & Madau, P. 2005, MNRAS, 363, 1069
Machacek, M. E., Bryan, G. L., & Abel, T. 2001, ApJ, 548, 509
———. 2003, MNRAS, 338, 273
Mizuta, A., Kane, J. O., Pound, M. W., Remington, B. A., Ryutov, D. D., & Takabe, H. 2005, ApJ, 621, 803
———. 2006, ApJ, 647, 1151
Oh, S. P., & Haiman, Z. 2003, MNRAS, 346, 456
O'Shea, B. W., Abel, T., Whalen, D., & Norman, M. L. 2005, ApJ, 628, L5
O'Shea, B. W., Bryan, G., Bordner, J., Norman, M. L., Abel, T., Harkness, R., & Kritsuk, A. 2004, preprint (astro-ph/0403044v1)
O'Shea, B. W., & Norman, M. L. 2007, ApJ, 654, 66
———. 2008, ApJ, 673, 14
Ricotti, M., Gnedin, N. Y., & Shull, J. M. 2001, ApJ, 560, 580
Schaerer, D. 2002, A&A, 382, 28
Shapiro, P. R., Iliev, I. T., & Raga, A. C. 1999, MNRAS, 307, 203
———. 2004, MNRAS, 348, 753
Susa, H. 2007, ApJ, 659, 908
Susa, H., & Umemura, M. 2006, ApJ, 645, L93
Whalen, D., Abel, T., & Norman, M. L. 2004, ApJ, 610, 14
Whalen, D., & Norman, M. L. 2006, ApJS, 162, 281
———. 2008a, ApJ, 672, 287
———. 2008b, ApJ, 673, 664
Williams, R. J. R. 2002, MNRAS, 331, 693
Wise, J. H., & Abel, T. 2007a, ApJ, 671, 1559
———. 2007b, ApJ, submitted (arXiv: 0710.3160v1)
———. 2007c, ApJ, submitted (arXiv: 0710.4328v1)
Yoshida, N., Oh, S. P., Kitayama, T., & Hernquist, L. 2007, ApJ, 663, 687